

Summer 1999

Designed Reduction of Radiated Noise Characteristics from Two-Bladed General Aviation Propellers

Chandra K. Stich

Embry-Riddle Aeronautical University - Daytona Beach

Follow this and additional works at: <https://commons.erau.edu/db-theses>



Part of the [Aerospace Engineering Commons](#), and the [Aviation Commons](#)

Scholarly Commons Citation

Stich, Chandra K., "Designed Reduction of Radiated Noise Characteristics from Two-Bladed General Aviation Propellers" (1999). *Theses - Daytona Beach*. 189.

<https://commons.erau.edu/db-theses/189>

This thesis is brought to you for free and open access by Embry-Riddle Aeronautical University – Daytona Beach at ERAU Scholarly Commons. It has been accepted for inclusion in the Theses - Daytona Beach collection by an authorized administrator of ERAU Scholarly Commons. For more information, please contact commons@erau.edu.

**Designed Reduction of Radiated Noise Characteristics from
Two-Bladed General Aviation Propellers**

by

Chandra K. Stich

A Thesis submitted to the
Department of Aerospace Engineering
in Partial Fulfillment of the Requirements for the Degree of
Master of Science in Aerospace Engineering

**Embry-Riddle Aeronautical University
Daytona Beach, Florida
Summer 1999**

UMI Number: EP31920

INFORMATION TO USERS

The quality of this reproduction is dependent upon the quality of the copy submitted. Broken or indistinct print, colored or poor quality illustrations and photographs, print bleed-through, substandard margins, and improper alignment can adversely affect reproduction.

In the unlikely event that the author did not send a complete manuscript and there are missing pages, these will be noted. Also, if unauthorized copyright material had to be removed, a note will indicate the deletion.

UMI[®]

UMI Microform EP31920
Copyright 2011 by ProQuest LLC
All rights reserved. This microform edition is protected against
unauthorized copying under Title 17, United States Code.

ProQuest LLC
789 East Eisenhower Parkway
P.O. Box 1346
Ann Arbor, MI 48106-1346

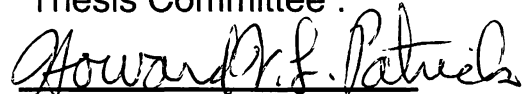
Designed Reduction of Radiated Noise Characteristics from Two-Bladed General Aviation Propellers

by

Chandra K. Stich

This thesis was prepared under the direction of the candidate's committee chair, Dr. Howard V.L. Patrick, Department of Aerospace Engineering, and has been approved by the members of this thesis committee. It was submitted to the Department of Aerospace Engineering and was accepted in partial fulfillment of the requirements for the degree of Master of Science in Aerospace Engineering

Thesis Committee :



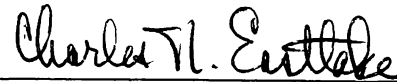
Dr. Howard V.L. Patrick
Chair



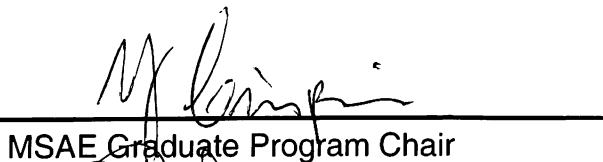
Dr. Yechiel Crispin
Member



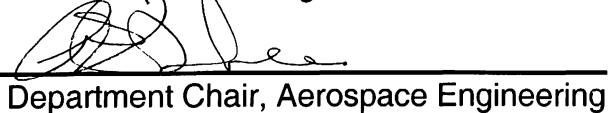
Dr. Don Higdon
Member



Professor Chuck Eastlake
Member



MSAE Graduate Program Chair



Department Chair, Aerospace Engineering

ACKNOWLEDGEMENTS

The author wishes to express sincere thanks and gratitude to Dr. Howard V.L. Patrick, Thesis Chair, whose never-ending encouragement, guidance and support were absolutely essential in the successful outcome of this thesis. Appreciation is also due to Drs. Crispin and Higdon, Thesis Committee Members, for their assistance in the preparation of this manuscript.

Additionally, a special thanks is given to the author's family and friends for their continual encouragement and assistance in the pursuit and completion of this thesis and in turn the degree of Masters of Science in Aerospace Engineering.

ABSTRACT

Author: Chandra Kay Stich
Title: Designed Reduction of Radiated Noise Characteristics from 2-Bladed General Aviation Propellers
Institution: Embry-Riddle Aeronautical University
Degree: Master of Science in Aerospace Engineering
Year: 1999

In recent years increased public awareness has made the reduction of environmental noise pollution a top priority for the aviation industry. Utilizing current technology, this study examines the reduction of noise generated by two bladed general aviation propellers, through design. The Aircraft Noise Prediction Program - Propeller Analysis System (ANOPP-PAS) is used to predict the noise and performance characteristics for an industry typical reference propeller as well as for the final quiet and efficient design.

This investigation is based on the use of a 200 hp engine rotating a 76 inch propeller. Typically, such a propeller would be rotated at 2700 rpm; however, the quiet propeller is designed to operate at 2400 rpm. This rotational velocity reduction is incorporated in order to decrease the rotational tip speed thereby preventing the formation of undesirable shocks at the tip. The reference propeller spinning at 2400 rpm achieves a 9 dB reduction in far field OASPL and a 9.6 (14 dBA) reduction in near field OASPL when compared to the reference propeller spinning at 2700 rpm. It should be noted that the values at 2700 rpm are under predicted by 3-10 dB due to a known ANOPP shortfall in shock wave noise prediction.

Blade twist distribution, tip shape, airfoil design, and blade sweep were all modified and examined through parametric study to further quiet the design and maintain desirable performance characteristics. These modifications produced additional reduction of 1.1dB (3.6 dBA) reduction in far-field OASPL. Near-field noise characteristics were reduced by 1.7 dB (2.3 dBA). The final quiet design is achieved with a 1% increase in performance.

Table of Contents

Acknowledgments	iv
Abstract	v
List of Tables	viii
List of Figures	ix
List of Symbols	xi
1.0 Introduction	1
1.1 Premise for Study	1
1.2 Review of Literature	3
2.0 Theory	6
2.1 Propeller Theory	6
2.2 Propeller Noise Theory	14
2.3 Noise Factors in Propeller Design	23
3.0 Analytic Methods	25
3.1 ANOPP-PAS	25
4.0 Propeller Design	29
4.1 Design and Analysis	29

Table of Contents Continued

4.2	Reference Propeller Definition	29
4.3	Reference propeller Aerodynamic Performance	36
4.4	Radiated Noise from Reference Propeller	38
4.5	Tip Shape	42
4.6	Propeller Rotational Speed (2400 vs. 2700 rpm)	45
4.7	In-Plane Sweep	48
4.8	Out-of-Plane Sweep	52
4.9	NLF Propeller	56
4.10	NLF Propeller Radiated Noise	60
4.11	Optimal Propeller Design	65
4.12	Unsteady Blade Loading	67
5.0	Conclusions	77
6.0	Recommendations	79
7.0	References	81

List of Tables

Table 4.2.1 Helix, Blade and Attack angles, chord c, and Sectional Lift Coefficient C_l as a Function of Radial Position r/R at a Design Advance Ratio of 1.07.	33
Table 4.4.1 Reference Propeller Near-field Thickness and Loading Noise as a Function of Harmonic Number at Directivity Angle 105°.	41
Table 4.5.1 Unweighted and A-weighted OASPL, Maximum Far-Field and Near-Field Levels at a Directivity Angle of 105°, for Different Propeller Tip Shapes.	43
Table 4.7.1 Maximum OASPL, Near and Far-Field, for all Blade Configurations.	52
Table 4.8.1 Maximum Far and Near Field OASPL for all Out-of-plane Swept Configurations	55
Table 4.9.1 Blade angles, chord and lift coefficient as a function of radial position for NLF propeller.	57
Table 4.10.1 Unweighted and A-weighted OASPL for Maximum Fly-Over and Near-Field Levels (at a Directivity Angle of 105°), for NLF and Reference Propeller's for straight, in and out-of-plane swept configurations.	63
Table 4.11.1 Unweighted and A-weighted OASPL for Maximum Fly-Over and Near-Field Levels (at a Directivity Angle of 105°), for the Reference, Straight NLF and the Optimal propellers.	67

List of Figures

Figure 2.1.1 Propeller in motion	6
Figure 2.1.2 Geometrical and effective pitch	7
Figure 2.1.3 Velocities and forces acting on a propeller blade	8
Figure 2.1.4 Typical Propeller Aerodynamic Performance	10
Figure 2.1.5 Propeller Airfoils Clark-Y, RAF- 6, Bottom NACA 16XX	13
Figure 2.2.1 Typical Propeller Noise Spectra	14
Figure 2.2.2 Gutin's polar Plot of Intensity	15
Figure 2.2.3 Components of Propeller Radiated Noise	19
Figure 2.3.1 Typical Propeller Blade Layout	23
Figure 3.1.1 ANOPP-PAS Noise Predictions vs. Test Data	26
Figure 4.2.1 NACA 4412 Sectional lift coefficient C_l vs. α	31
Figure 4.2.2 Sketch of the reference propeller blade	32
Figure 4.2.3 Reference propeller Beta vs. r/R	35
Figure 4.3.1 Aerodynamic Performance (Reference Propeller)	37
Figure 4.4.1 Near-Field OASPL as a function of directivity	38
Figure 4.4.2 Sketch of Directivity angle γ.	39
Figure 4.4.3 Near-Field Noise vs. Harmonic # Reference Prop.	40
Figure 4.4.4 Far-field Noise Reference Propeller @ 2400 RPM	42
Figure 4.6.1 Far-Field OASPL of Ref. Prop. at 2400 and 2700 rpm	46
Figure 4.6.2 Near-Field SPL (Ref. Prop.) Rotating at 2400 and 2700	47
Figure 4.7.1 Planform View of In-plane Swept Blade Configurations	50

List of Figures Continued

Figure 4.7.2 Far-field OASPL of HIPSE 6.5 and Reference Propeller	51
Figure 4.8.1 Far-field OASPL of OPSE 6.5 and Reference Propeller	54
Figure 4.9.1 NACA 44 and NLF series airfoils	58
Figure 4.9.2 Performance of Propeller with NLF Airfoils	59
Figure 4.10.1 Fly-over OASPL Far-Field Radiated Noise Characteristics of Straight NLF and Reference Propellers	61
Figure 14.10.2 Frequency Distribution of Near-Field SPL for the NLF Propeller and the Reference Propeller rotating at 2400 RPM	62
Figure 4.11.1 Fly-over Unweighted OASPL Far-Field Radiated Noise Characteristics of the Reference and Optimal Propellers	66
Figure 4.12.1 Comparison of Unsteady and Steady Far-Field Radiated Noise	69
Figure 4.12.2 Comparison of Unsteady and Steady Overall Noise generated by Reference Propeller [SPL vs. Harmonic Number (f)]	71
Figure 4.12.3 Comparison of Unsteady and Steady Thickness Noise from the Reference Propeller [SPL vs Harmonic Number (f)]	72
Figure 4.12.4 Comparison of Unsteady and Steady Loading Noise from the Reference Propeller [SPL vs Harmonic Number (f)]	73
Figure 4.12.5 Unsteady and Steady Directivity Patterns [Near-Field OASPL as a function of Directivity Angle]	74
Figure 4.12.6 Comparison of Unsteady and Steady Far-Field Radiated Noise At 1000ft	76

List of Symbols

<p>AF = activity factor</p> <p>b = chord length</p> <p>B = number of blades</p> <p>BPF = blade passing frequency</p> <p>c = speed of sound</p> <p>c_l = lift coefficient</p> <p>C_{lmax} = maximum sectional lift coefficient</p> <p>C_p = power coefficient</p> <p>C_T = thrust coefficient</p> <p>dB = decibel</p> <p>dBA = A-weighted decibel</p> <p>D = diameter; drag</p> <p>FW-H = Ffocws Williams – Hawkings Equation</p> <p>J = propeller advance ratio</p> <p>J_{mB} = Bessel function</p> <p>k = wave number; correction factor for finite solidity</p> <p>L = lift</p> <p>\dot{L}_i = rate of change of the force</p> <p>M = source mach number.</p> <p>M_r = source Mach number component in direction of radiation vector</p> <p>n = rotational speed; blade number</p> <p>NLF = natural laminar flow</p> <p>OASPL = overall sound pressure level</p> <p>p = acoustic pressure</p> <p>P = power</p> <p>P_{ij} = compressive stress tensor</p> <p>Q = torque</p> <p>\hat{r} = unit vector from source point at emission time to observer</p> <p>R = radius; distance from source at emission to observer</p> <p>s = solidity</p> <p>SPL = sound pressure level</p> <p>t = blade thickness</p> <p>T = thrust</p> <p>T_{ij} = turbulence stress tensor</p> <p>V_o = free stream velocity</p> <p>V_t = tangential component of rotational speed</p>	<p>α = angle of attack</p> <p>α_i = induced angle of attack</p> <p>β = blade angle; geometric pitch</p> <p>γ = directivity</p> <p>$\delta(f)$ = dirac delta</p> <p>η = propeller efficiency</p> <p>v_n = local normal velocity of blade surface</p> <p>Φ = helix angle of advance</p> <p>Φ_o = effective helix anle</p> <p>Φ_{mB} = velocity potential</p> <p>ρ = air density</p> <p>σ = solidity</p> <p>ω, Ω = rotational speed</p> <p>∇ = gradient</p> <p>∇^2 = Laplacian operator</p> <p>\diamond^2 = wave operator</p>
--	---

1.0 Introduction

1.1 Premise of Study

Aircraft noise has significant effects on the world community. These effects range from slight annoyance to severe physical and psychological problems for those who live, and work near airports. Community members often find that the noise from aircraft interferes negatively with their daily lives; reducing productivity, rest and sleep. Aircraft certification requires compliance with current noise regulations, as defined in FAA FAR Part 36. However, many local communities are pressuring the government for stricter regulations. The US has literally thousands of small local airports and as the aviation community expands these once accepted airports often find themselves in a noise controversy where aviators and community residents collide. The European community has similar conflicts; however, their problems are greatly magnified due to significantly higher population densities. In fact, the number of licensed general aviation pilots in Europe has already been restricted and additionally European communities are forcing such heavy restrictions that the recreational pilot is becoming significantly threatened.

Acoustic efficiency is inherently desirable in general aviation technology. That is, noise is caused by a considerable loss of energy and the minimization of this noise is thus, required for optimal design. This fact coupled with pressure from the world community to reduce noise pollution has sparked a quest for improvement in acoustic efficiency in the worlds general aviation market. Operating hour restrictions of airports have helped to lessen community

concerns, but now real solutions to noise abatement must be found and implemented. Reduction in the overall noise caused by general aviation aircraft will benefit the aviator, who is constantly surrounded by noise radiation. The noise within the cabin of general aviation aircraft is significant, as is witnessed by all small aircraft occupants, the noise may in time prove hazardous to those constantly exposed. Additionally acoustic emissions can cause the aircraft structure to fatigue over time, due to constant acoustically induced vibration during propeller operation. Thus, study of propeller noise reduction should focus not only on far-field radiation that effects entire communities, but additionally it should encompass near field acoustic emissions.

Propeller driven aircraft noise is dominated by propeller tip speed, propeller blade tip thickness, and engine exhaust system characteristics. Thus, the propulsion system must be designed with considerable thought given to these parameters, with special attention given to climb and fly-over noise. Analysis of current general aviation aircraft estimates that approximately 84 percent of noise is directly traceable to the propeller [1]. Propeller radiated noise can be suppressed in several ways including passive noise control at the receiver, optimally syncrophazing propellers on multi-engine aircraft, and active noise control at the source and receiver. All of the previously mentioned methods are successful to varying extents. Though significantly different methods, they all have one thing in common, they reduce propeller noise after it is generated. Perhaps the best way to reduce propeller noise is to prevent its generation. Although optimal acoustic design can not eliminate acoustic emissions of the propeller, an optimal design can minimize the propellers overall

acoustic emissions and in various ways, the reduction of propeller noise has been previously undertaken. [2]

1.2 Review of Literature

Initial noise reduction investigations of propeller driven aircraft were led by military groups seeking to reduce detectability of their aircraft. Small sources by comparison, propeller driven aircraft noise was somewhat set aside in the early age of the jet. Since the 1970's, increased public awareness of noise pollution's adverse effects has forced the aviation industry to re-examine noise issues. In 1977, the FAA in conjunction with the EPA began regulating aviation noise, airport noise abatement features, and airport noise planning. [3] However in an effort to seek further noise reduction those concerned with aviation generated noise pollution, sought to prevent the origination of the noise at its' source. General aviation aircraft noise has three main elements consisting of: propeller generated noise (84%), exhaust noise (2%) and exhaust propeller combinations and unidentified sources (14%)[1]. Two-bladed fixed pitch propellers have a limited number of noise reduction techniques that can be implemented through the design phase: reducing RPM, reducing propeller diameter, utilizing in and out of plane sweep, changing tip geometry, and using high performance airfoils. Over the years, each of these parameters have been examined in an effort to reduce the noise generated by general aviation propellers. In the late seventies Davis studied the impact of using airfoils with performance better than that achieved with NACA 16 and 65 airfoils. [2] These higher performance airfoils increased blade loading such that performance is maintained at lower rpm thereby reducing

noise. A 200 rpm reduction in rotational speed was predicted to provide a 3 dB reduction in far-field radiated noise. [2]

Klatte and Metzger studied the impacts to noise emission when the design parameters were modified in three different aircraft propellers (1970-1981). [3] One of the Klatte and Metzger investigations focused on a single engine Debonair. Tip shape modifications, replacing RAF-6 airfoils with NACA 16 airfoils and changing the twist distribution resulted in 7.0 dBA reduction in far-field radiated noise characteristics. Further investigations of blade sweep in the Debonair study indicated that high levels of tip sweep (52 deg.) resulted in high amounts of noise reduction (5.5 dBA). [4] In 1980 Korkan studied the noise radiation impacts when propeller sweep was modified on four different aircraft. [3] The Korkan study indicated that when a propeller has medium to high tip loading, incorporation of sweep reduces the radiated noise characteristics.

All of the aforementioned design parameters have varying potential to provide noise reduction benefits. [4] Reduction in RPM with blade optimized for slower rotational speed has a high potential for noise reduction (5-8 dBA); however, there is some concern for structural reliability due to high twist needed in blade design and unknown installation effects. Changing of tip geometry has a low to medium predicted effect on noise reduction potential (1-5 dBA), depending on tip design there are potential structural limitations as well as potential production cost impacts. The use of high performance airfoils has low potential of achieving noise reduction (1-3 dBA) however performance may be increased when incorporated into design. Sweeping the propeller tip currently has a low

potential for noise reduction (1-3 dBA), this benefit could be increased with high amounts of sweep; however, sweep incorporation is limited by structural reliability and production cost increases.

Leaps in current material technology and manufacturing processes will allow propeller designs to incorporate relatively thin airfoils. [4] Improvements in manufacturing will also allow propellers to be designed with increasing blade angles, which provide high aerodynamic efficiency and ultimately improved acoustic efficiency. Incorporation of in-plane sweep will also become increasingly possible resulting in reduction of far-field noise due to cancellation of the distributed load. The use of out-of plane sweep in GA propeller design will also become easier to incorporate with better materials and manufacturing processes and incorporation will decrease near-field noise radiation at cruise. [1] Thus, two-bladed fixed pitch propeller noise radiation can be decreased through fundamental changes in design without sacrificing propeller performance. In this study all of the aforementioned design parameters will be examined, optimized, and combined to create a propeller that has superior aerodynamic and aeroacoustic efficiency.

2.0 Propeller Theory

2.1 Propeller Aerodynamic Theory

Propellers are designed to provide thrust for aircraft by imparting a relatively small increase in velocity to a relatively large mass of air. Aerodynamic propeller blades act much like small wings. Each blade has a normal type airfoil section that derives its propulsive forces from the airflow passing over it.

Figure 2.1 illustrates a propeller in motion.

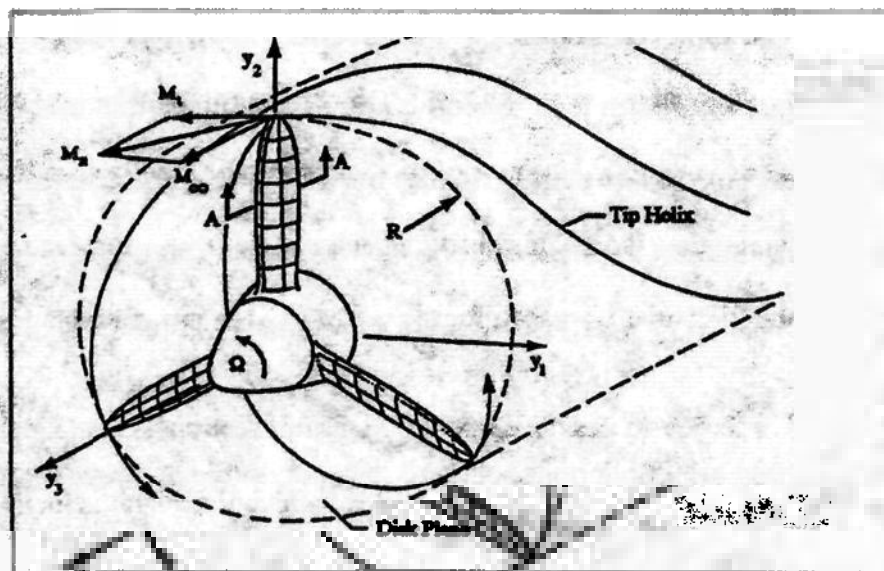


Figure 2.1.1 Propeller in motion. [5]

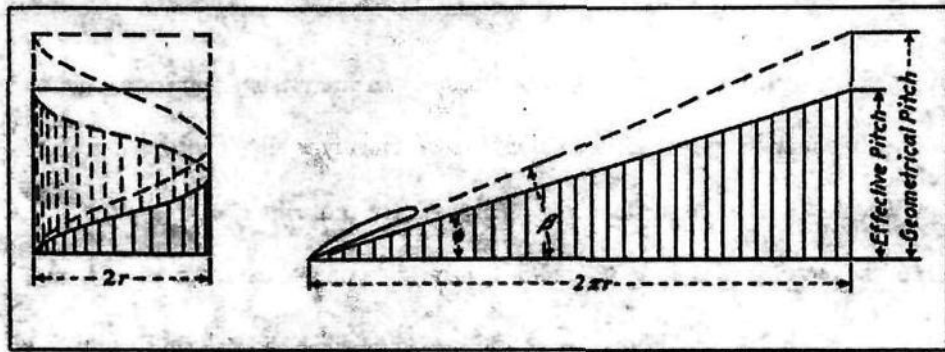


Figure 2.1.2 Geometrical and effective pitch. [7]

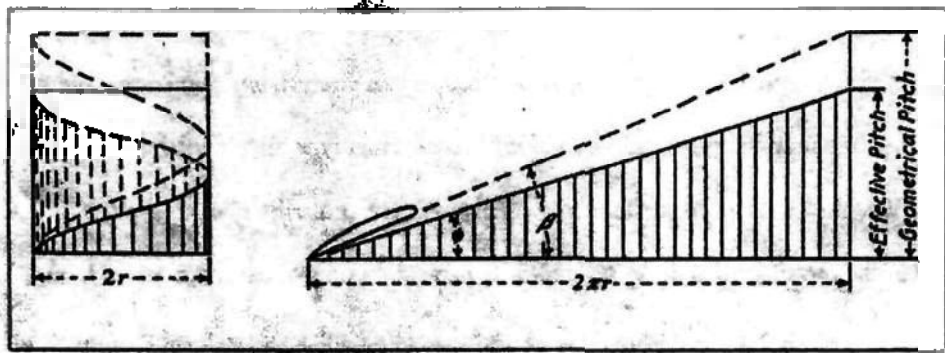


Figure 2.1.2 Geometrical and effective pitch. [7]

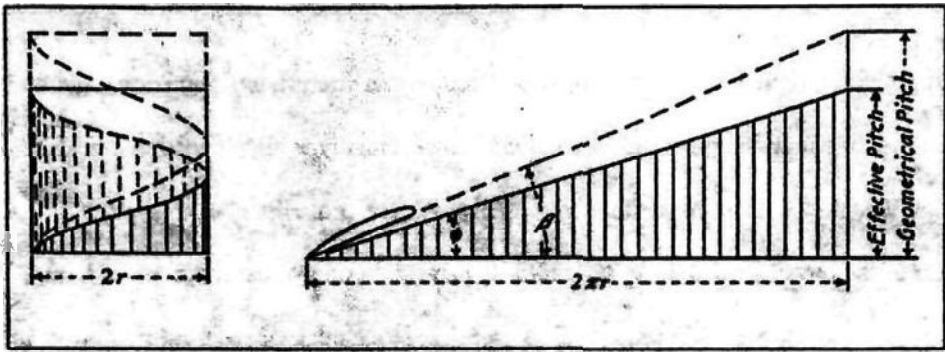


Figure 2.1.2 Geometrical and effective pitch. [7]

Figure 2.1.3. Pitch angle effects the blade loading thus, it is also an important factor in the propeller design.

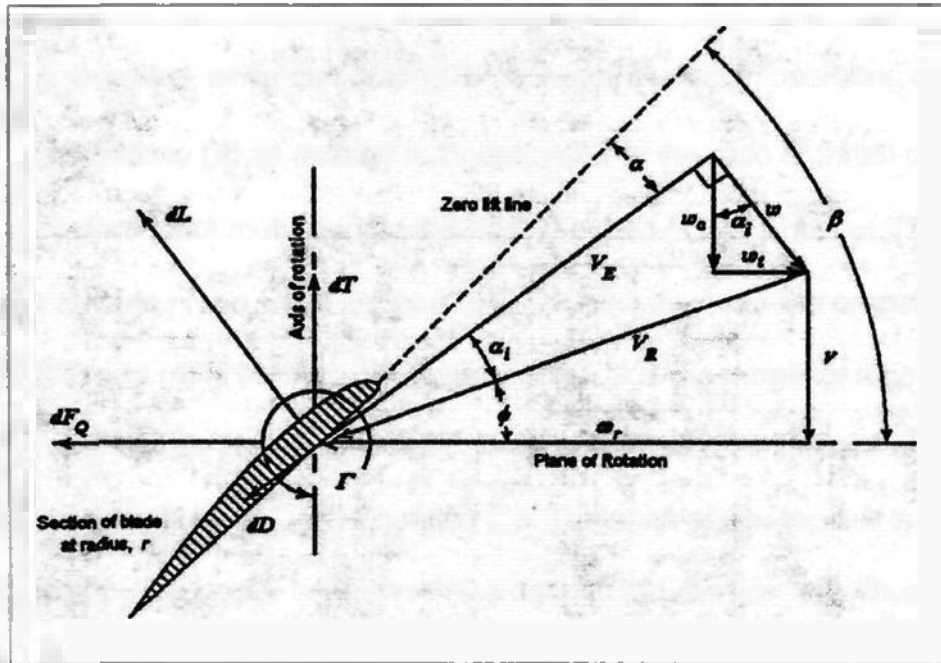


Figure 2.1.3 Velocities and forces acting on a propeller blade cross section [5].

The lift to drag ratio (L/D) of the airfoil section is a function of the angle of attack. The thrust to torque ratio (T/Q) is also a function of angle of attack and therefore the L/D ratio. However, the T/Q ratio is also a function of the helix angle. This causes considerable changes in the T/Q ratio along the span of the blade. [7] Thus, the pitch angle will affect the design of the blade, and since pitch angle is a function of helix angle, the twist becomes an important aspect, in that it controls the pitch angle distribution. The ideal condition for high propeller efficiency requires the optimum angle of attack be achieved along all of the blade sections. The optimal angle is achieved through the propeller blade twist as

previously discussed. The twist distribution controls how the optimum angle of attack varies along the span of the blade.

The propeller blade design should produce the maximum aerodynamic efficiency possible, while conforming to the required design operating conditions. Propeller efficiency (η) as defined in Equation 2.1 is the ratio of thrust output to the shaft power input multiplied by the advance ratio of the propeller. [7] The propeller advance ratio (J), is defined in Equation 2.2. where the propeller rotational speed (n) is in revolutions per second, D is the propeller diameter and V_0 is the aircraft free-stream velocity. [7] The power output is defined by thrust (T) or the thrust coefficient (C_T) in Equation 2.3. The shaft power input P is represented by the power coefficient (C_P) defined in Equation 2.4. Thus, propeller efficiency is dependent on the forward speed, diameter, propeller rotational speed and the ratio of thrust output to shaft power input.[7].

$$\eta = (C_T/C_P)J \quad \text{Equation 2.1}$$

$$J = V_0/nD \quad \text{Equation 2.2}$$

$$C_T = T/\rho n^2 D^4 \quad \text{Equation 2.3}$$

$$C_P = P/\rho n^3 D^5 \quad \text{Equation 2.4}$$

Figure 2.4 shows the typical aerodynamic characteristics for a sample propeller, where the thrust coefficient C_T , the power coefficient C_p and efficiency η are plotted as a function of advance ratio J .

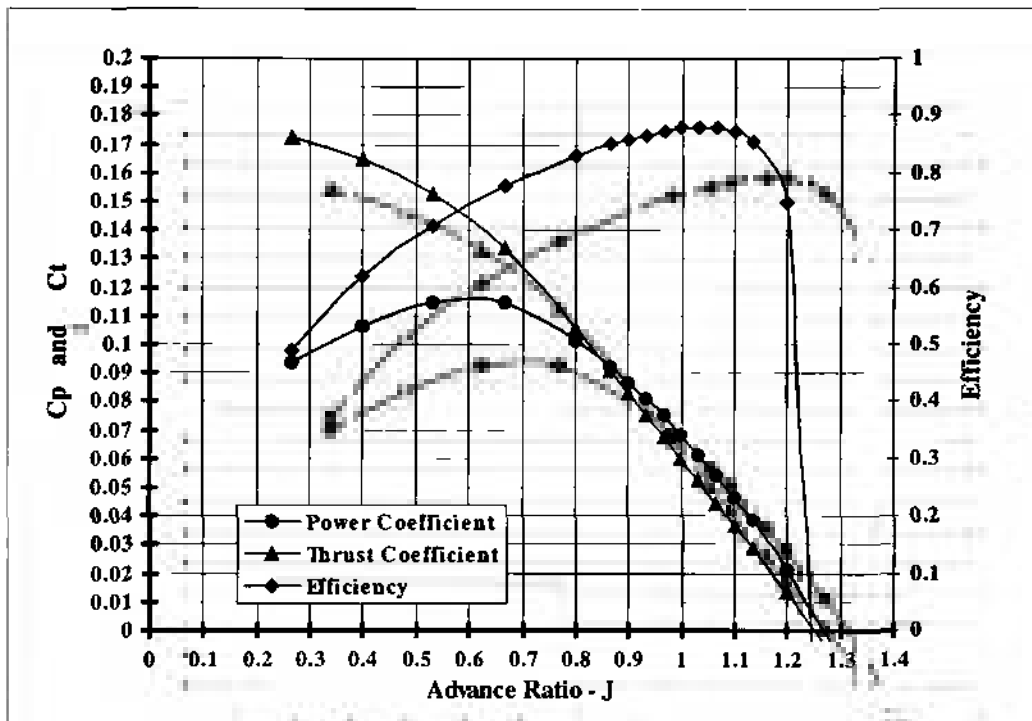


Figure 2.1.4 Typical Propeller Aerodynamic Performance Characteristics [6].

Each engine has a definite revolution speed that provides the optimal combination of thrust and power and thus, the maximum efficiency. [8] Varying the aerodynamic qualities of the propeller blade will lead to varying levels of propeller efficiency. Thus, it is important to know what these factors are and understand how they affect the propeller's performance in order to design efficient propellers.

Blade diameter, total planform area, airfoil section and twist are the most important factors to consider when designing the propeller. One particular combination of diameter and pitch will give the aircraft its maximum speed. Similarly, other combinations of pitch and diameter will give the conditions for the best rate of climb, the best departure and climb angle or the best cruising speed. Departure and climb performance are considered to be equally important to cruising speed and maximum speed, therefore a compromise of these parameters is sought in the design general purpose propellers. [8] When the aircraft is sitting on the runway its advance ratio J is zero and J increases as the propeller begins to move forward. It is important that C_T be sufficiently high to insure good take off performance. Generally, for constant pitch propellers, low J tends to be the least efficient phase of operation due to separated flow. Several fundamental limits must be established for the propeller design: ground clearance required, structure interference limits, potential interference with other propellers, and the propellers slipstream. The forward speed, altitude and rotational speed can also limit the propeller diameter. [7] Blade number is generally effected by considerations of optimal propeller efficiency.

Other factors affecting the efficiency of propeller design are the blade width, thickness ratio, the blade section or airfoil, blade solidity, the plan form and the activity factor. Blade solidity σ is defined as the ratio of total blade area to propeller disk area, solidity it is used to determine the capability of a propeller to absorb power. [9]

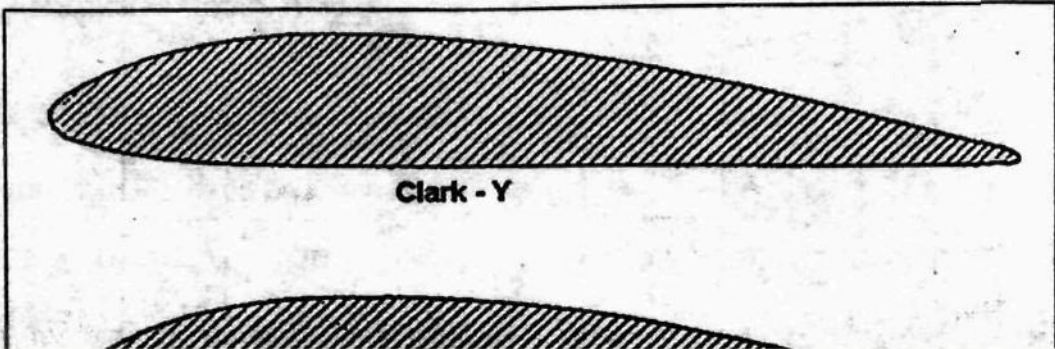
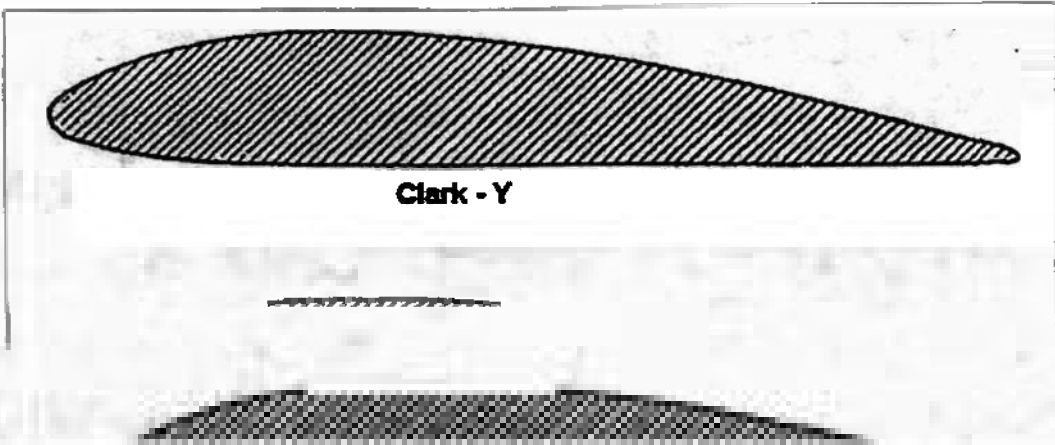
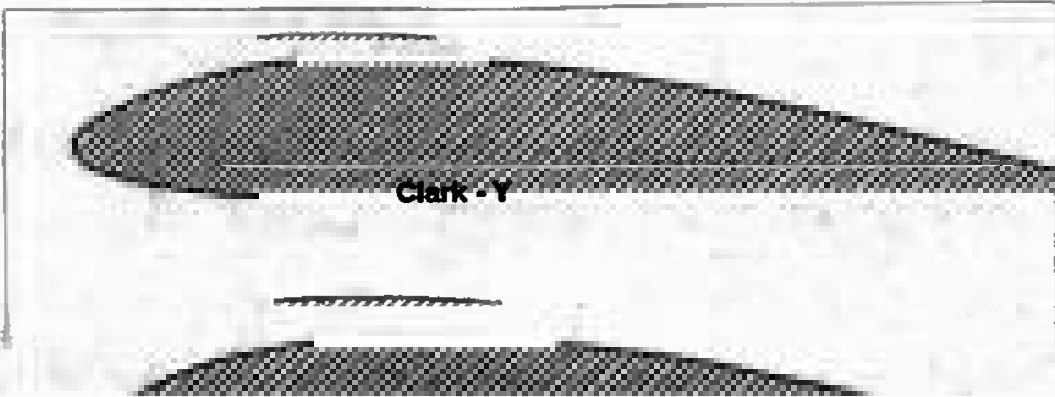
Activity factor (AF) determines the amount of power absorbed by the propeller under specific operating conditions and is defined in Equation 2.5. [10]

$$AF = \frac{100,000}{16} \int_{0.2}^{1.0} \left(\frac{b}{D} \right) \left(\frac{r}{R} \right)^3 d \left(\frac{r}{R} \right)$$

Equation 2.5

Where b is the blade width at radius r , R is the propeller radius and D is the propeller diameter. Thus, AF utilizes blade width distribution between the hub and tip to determine the propellers ability to absorb power.

Illustrated in Figure 2.1.5, are the most common airfoil sections used in propeller design the RAF 6, Clark Y and NACA 16 series. In more recent years supercritical airfoil sections have also been used. It is also advisable to use laminar flow airfoil sections to minimize the losses in efficiency due to compressibility. Compressibility is one of the factors that affect instability and the transition from laminar to turbulent flow. Turbulent flow over the propeller surface will reduce the propeller's aerodynamic efficiency and thus its aeroacoustic efficiency. Laminar flow airfoils are designed to give constant velocity distribution across the chord under the required design operating conditions.



2.2 Propeller Noise Theory

Propeller noise is characterized by tones that occur at blade passing frequency (BPF) and its harmonics. Blade passing frequency is the frequency at which a blade passes a fixed point in the propeller's plane of rotation and is a function of blade number n and rotational speed of the propeller Ω as shown in

2.2 Propeller Noise Theory

Propeller noise is characterized by tones that occur at blade passing frequency (BPF) and its harmonics. Blade passing frequency is the frequency at which a blade passes a fixed point in the propeller's plane of rotation and is a function of blade number n and rotational speed of the propeller Ω as shown in

2.2 Propeller Noise Theory

Propeller noise is characterized by tones that occur at blade passing frequency (BPF) and its harmonics. Blade passing frequency is the frequency at which a blade passes a fixed point in the propeller's plane of rotation and is a function of blade number n and rotational speed of the propeller Ω as shown in

2.2 Propeller Noise

Discrete tones or rotational noise is caused by the periodic disturbance of the air as the propeller blade rotates. The sources of this noise are the steady forces of thrust and torque which act on the blades. Each element of the propeller blade has a pressure distribution due to its motion through the air. This distribution can be resolved into thrust and torque force components. The

Discrete tones or rotational noise is caused by the periodic disturbance of the air as the propeller blade rotates. The sources of this noise are the steady forces of thrust and torque which act on the blades. Each element of the propeller blade has a pressure distribution due to its motion through the air. This distribution can be resolved into thrust and torque force components. The

Discrete tones or rotational noise is caused by the periodic disturbance of the air as the propeller blade rotates. The sources of this noise are the steady forces of thrust and torque which act on the blades. Each element of the propeller blade has a pressure distribution due to its motion through the air. This distribution can be resolved into thrust and torque force components. The

Discrete tones or rotational noise is caused by the periodic disturbance of

Gutin was the first propeller noise theorist to recognize the dipole nature and the directional properties of propeller noise as shown in Figure 2.2.2. [13]. In the 1930's, he developed the first successful theory of propeller radiated noise. Gutin assumed that the propeller blade width was very small and that the excitation could be treated as an impulse function. This fundamental assumption allows that the amplitude of the harmonics to be constant and a relation for torque and thrust can then be determined. [13,14]

The total velocity potential can be obtained from Equation 2.2.1 when the forces, the velocity potential (Φ_{mB}) produced by a concentrated force and the geometry to the observer can be determined. The sound pressure (p_{mB}) is given by Equation 2.2.2.

Equation 2.2.1

$$\Phi_{mB} = \frac{e^{ik(ct-r_o)}}{4\pi^2 \rho c r_o} \iint \left\{ \frac{dT}{dR} \cos \delta + \frac{1}{R} \frac{dQ}{dR} \sin \delta \sin \Theta \right\} e^{i(\sin \delta \cos \Theta - mB\Theta) dR d\Theta}$$

Equation 2.2.2

$$p_{mB} = \frac{mB\Omega}{2\pi c r_o} \int_0^{R_r} \left\{ -\frac{dT}{dR} \cos \delta + \frac{c}{\Omega R^2} \frac{dQ}{dR} \right\} J_{mB}(kR \sin \delta) dR$$

This sound pressure is the RMS value of pressure in the far-field at a distance r_0 and position in space defined by angles δ , and Θ for the n th harmonic of BPF for a single propeller [12]. Where m is the order of the harmonic, B is the number of blades, Ω is the angular velocity of rotation, c is the speed of sound, R is the radius of the element considered, dT/dR is the thrust gradient along the radius, dQ/dR is the torque distribution, k is the wave number of the m th harmonic and J_{mB} is a Bessel function of the first kind.

The noise caused by the thickness of the blade is the other component of rotational noise. The noise is caused by an element of air being physically displaced by the rotating propeller. A finite volume of air is displaced by the rotating propeller, and it may be represented as a monopole, the strength determined by the component of displacement velocity normal to the propeller plane. Thickness noise has the same BPF and harmonics as loading noise and at high tip speeds thickness noise is a significant component of the overall noise generated by the propeller.

An expression for the far-field noise due to thickness is expressed in equation 2.2.3.

Equation 2.2.3

$$P'_{mB} = \frac{\rho B \omega^2}{(2\sqrt{2})\Pi r_o} \int ktb J_{mB}(kR \sin \delta) dR$$

In Equation 2.2.3, ρ is air density, ω is the rotational speed, k is a correction factor for finite solidity and t is the thickness and b is the chord length at radius R .

The second type of noise is broadband or vortex noise. Unlike the rotational noise, broadband noise is the effect of random, fluctuating disturbances which may be initiated at the propeller. The sources of broadband noise include the turbulent regions in the propeller blade wake. Vortex shedding produces fluctuating forces that interact with the trailing edge of the propeller blade.

Broadband noise is generally significantly less than discrete noise and can be neglected. However, if any portion of the propeller blade is stalled, broadband noise can become a significant contributor to the sound spectrum. The nonlinear quadrupole noise can be used to describe all viscous and propagation effects not covered by loading and thickness sources. Generally however the quadrupole source is most practically used to evaluate non-viscous flow close to the blade surface. At transonic section speeds of unswept, high tip-speed propellers, the quadrupole increases the loading and thickness noise sources. Figure 2.2.3 illustrates the various types and classifications of the aforementioned propeller noise components.

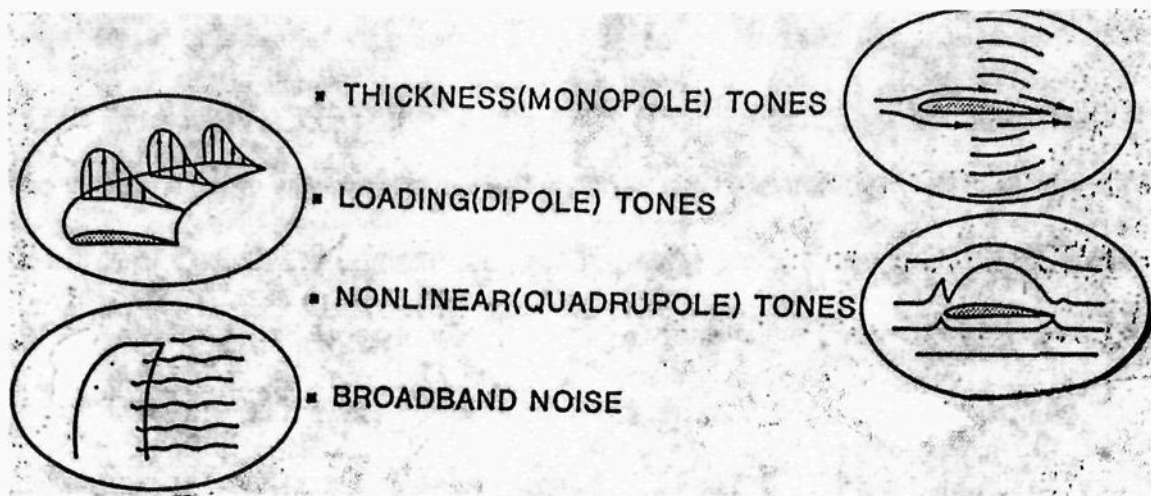


Figure 2.2.3 Components of Propeller Radiated Noise. [11]

In 1969 J.E. Ffowcs Williams and D.L. Hawkings [15] generalized Lighthill's [16] results to a blade surface in motion, with quadrupoles around the surface and thickness and loading sources on the surface itself. They were still working with a quiescent medium and the results of their work is referred to as the Ffowcs Williams - Hawkings (FW-H) equation. [14] The key to applying the FW-H equation to propeller noise, is neglecting the second order source term that depends on Lighthill's stress tensor. [12] This results in a usable equation that is valid and can be solved using Green's functions for unbounded space.

The FW-H equation is based on the conservation of momentum and mass. Williams and Hawkings [12,14] established the original derivation, and Farassat [12] introduced the embedding process. This process results in an equation that is useful for computational aeroacoustics and generates theoretical values that compare reasonable well with experimental data. The result gives an

equation that is useful for computational aeroacoustics and generates theoretical values that compare reasonably well with experimental data. The FW-H equation considers a body whose surface is described by the equation $f(x, t) = 0$ where the x-frame is fixed to the undisturbed medium and t represents time. The equation of the surface $f = 0$ is defined such that $f > 0$ is outside the body and $f < 0$ inside the body. The general Ffowcs-Williams Hawkins equation to determine acoustic pressure for a surface is given by equation 2.2.4. [14]

Equation 2.2.4

$$\diamond^2 p = \frac{1}{c^2} \frac{\partial^2 p}{\partial \tau^2} - \nabla^2 p = \frac{\partial}{\partial \tau} \{ \rho_0 v_n |\nabla f| \delta(f) \} - \frac{\partial}{\partial y_i} \left[P_{ij} \frac{\partial f}{\partial y_j} \delta(f) \right] + \frac{\partial^2 T_{ij}}{\partial y_i \partial y_j}$$

In equation 2.2.4, p is the acoustic pressure, ρ_0 and c are the density and speed of sound of the undisturbed medium, respectively, v_n is the local normal velocity of the blade surface, $\delta(f)$ is the dirac delta function, \diamond^2 denotes the wave operator. ∇^2 is the Laplacian operator and ∇f is the gradient of the function defining the blade surface. Surface pressure and viscous stress are represented by $\partial p^2 / \partial \tau^2$. The compressive stress tensor is represented by the P_{ij} term and is the force acting on the fluid due to surface pressure distribution and viscous stress on the surface of the body. The source terms of the right hand side of the

equation are known as the thickness, loading and quadrupole terms respectively. The stress tensor term T_{ij} is a quadrupole noise source that represents noise due to turbulence. This broadband turbulent noise source is generally much lower than the discrete noise and can be neglected. Neglecting the quadrupole terms gives equation 2.2.5 where \hat{n}_i is the unit outward normal to the body. [14]

Equation 2.2.5

$$\diamond^2 p = \frac{\partial}{\partial \tau} \{ p_o v_n |\nabla f| \delta(f) \} - \frac{\partial}{\partial y_i} [p \hat{n}_i |\nabla f| \delta(f)]$$

Using equation 2.2.5, Formulation 1A was developed by F. Farassat [15] as an integral representation of the FW-H equation. When given the body geometry, motion and surface loading, this formulation becomes a solution to the FW-H equation and acoustic problems. The NASA propeller prediction program ANOPP-PAS, which will be used to predict propeller noise, uses Formulation 1A.

Formulation 1A is valid for arbitrary blade motion and geometry. The sources lie on the actual body surface and can include loading from any mechanisms that act on the blade surface. Near-field and far-field terms are $1/r$ and $1/r^2$ terms respectively. The observer is fixed to the undisturbed medium. [15] To derive the formulation 1A, the equation needs to be converted from a Cartesian ground-fixed frame of reference to a blade-fixed frame. The formal

solution to the wave equation is used to give the integral representation of the FW-H equation. After several conversions and transformations, the final result is given by Equation 2.2.6. [14] Equation 2.2.7 denotes the loading and thickness noise and equation 2.2.8 denotes the total noise neglecting the quadrupole terms.

Where:

R is the distance from source point at emission time to observer,

M_r is the source Mach number component in the direction of the radiation vector,

\hat{r} is the unit vector from source point at emission time to observer,

\dot{l}_i is the rate of change of the force per unit distance (time derivative) as observed from the ground fixed frame,

M is the source mach number.

Equation 2.2.6

$$4\pi p'_L(\vec{x}, t) = \frac{1}{c} \int_{f=0} \left[\frac{\dot{l} \cdot \hat{r}}{r(1-M_r)^2} \right]_{\tau} dS + \int_{f=0} \left[\frac{l_r - l_i M_i}{r^2(1-M_r)^2} \right]_{\tau} dS + \frac{1}{c} \int_{f=0} \left[\frac{l_r (r\dot{M}_i \hat{r}_i + cM_r - cM^2)}{r^2(1-M_r)^3} \right]_{\tau} dS$$

Equation 2.2.7

$$4\pi p'_T(\vec{x}, t) = \int_{f=0} \left[\frac{\rho_o v_n (r\dot{M}_i \hat{r}_i + cM_r - cM^2)}{r^2(1-M_r)^3} \right]_{\tau} dS$$

Equation 2.2.8

$$p'(\vec{x}, t) = p'_L(\vec{x}, t) + p'_T(\vec{x}, t)$$

2.3 Noise Factors in Propeller Design

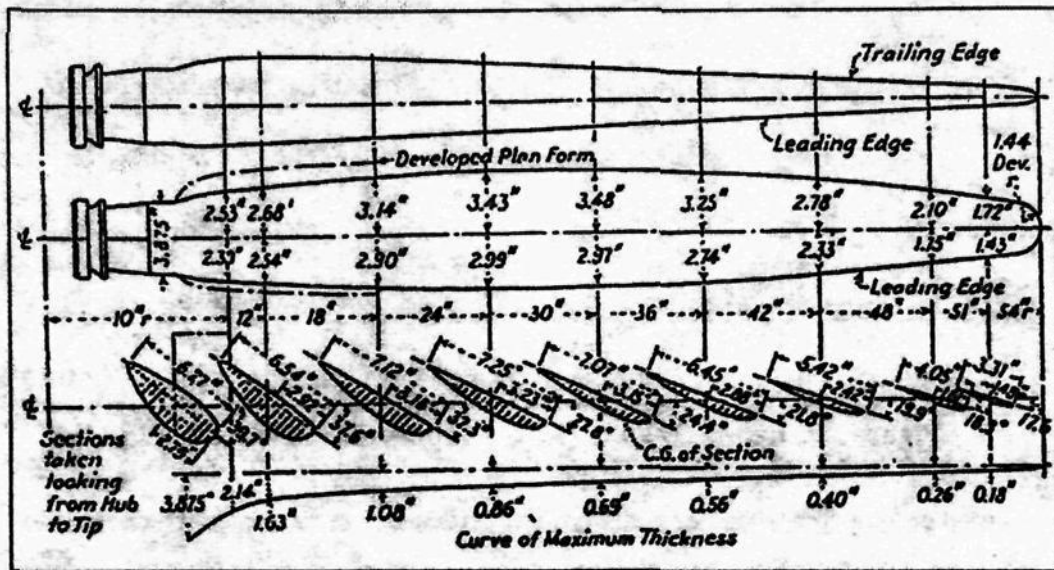


Figure 2.3.1 Typical Propeller Blade Layout [7]

The geometric and aerodynamic characteristics of a propeller are fundamentally linked to the noise generated by the propeller; shown in Figure 2.3.1 is the typical layout of a propeller blade. Operating conditions and environment, blade number, tip speed, torque, thrust, and blade thickness all affect the noise produced by the propeller. Propeller generated noise can thus be controlled through the manipulation of the propeller's design parameters. Noise reduction can be achieved by minimizing source contributions, thus the propeller designer must have a fundamental knowledge of the acoustic sources of propeller noise.

Broadband propeller noise occurs as a random source. Broadband reduction can be accomplished through sweeping the propeller's trailing edge [17]. This is possible because the velocity component normal to the trailing edge is reduced thereby reducing the noise generated by vortex shedding.

Because tonal noise is the largest contributor to the overall noise generated by the propeller, most reduction efforts focus on it. Discrete frequencies of a propeller occur as peaks at blade passing frequency (BPF) and its harmonics. The peaks can then be divided into loading and thickness noise components. The propeller thrust and torque create loading noise, while the volume of air displaced by the propeller blade generates thickness noise. Loading noise can be modified through alteration of tip speed, thrust, blade number, torque, pressure and loading distributions of the propeller. Decreasing the volume of the propeller's airfoil sections can minimize thickness noise. When attempting to design a quiet propeller blade it is important to avoid stall on the propeller blade because stall can increase both broadband and discrete generated noise. Stall increases discrete levels at BPF and its harmonics and also results in high levels of broadband noise. Stall can be induced on a propeller if loading is excessively high thereby causing flow separation on all or part of the blade. [16]

3.0 Analytic Method

3.1 ANOPP-PAS

NASA's Aircraft Noise Prediction Program Propeller Analysis System (ANOPP-PAS) is usually used as an aeroacoustic prediction code and not as a propeller design tool. However for this study it is used as a fundamental tool in the propeller design process. ANOPP-PAS is unique in that it allows the designer to reliably predict propeller performance and noise characteristics in the conceptual design phase. Thus, ANOPP-PAS is used in this study to achieve an optimum propeller design without having to fabricate or test an actual propeller.

ANOPP-PAS was developed over a twenty-year period beginning in 1976 and predicts the source noise, performance, propagation effects and response of propellers. ANOPP-PAS makes aeroacoustic and aerodynamic predictions for propellers in wind tunnel and flight conditions, and predicts propeller noise for both near and far-field acoustic radiation.

ANOPP-PAS prediction techniques include performance (PRANDTL-BETZ Vortex theory), source noise (Farassat Solution to FW-H equation), ground effects (Chien-Soroka), and atmospheric absorption (ANSI Standard). [11]

ANOPP-PAS data correlates well with data from propellers in flight and in wind tunnel experiments [18]. For example, ANOPP-PAS predictions match almost identically with FAA/DFLVR DNW test data shown in Figure 3.1.1 [18]. Also, when ANOPP-PAS data is compared to actual FAA fly-over data of a Piper Lance Aircraft it is apparent that ANOPP is a reliable and remarkably accurate prediction code as shown in Figure 3.1.1.

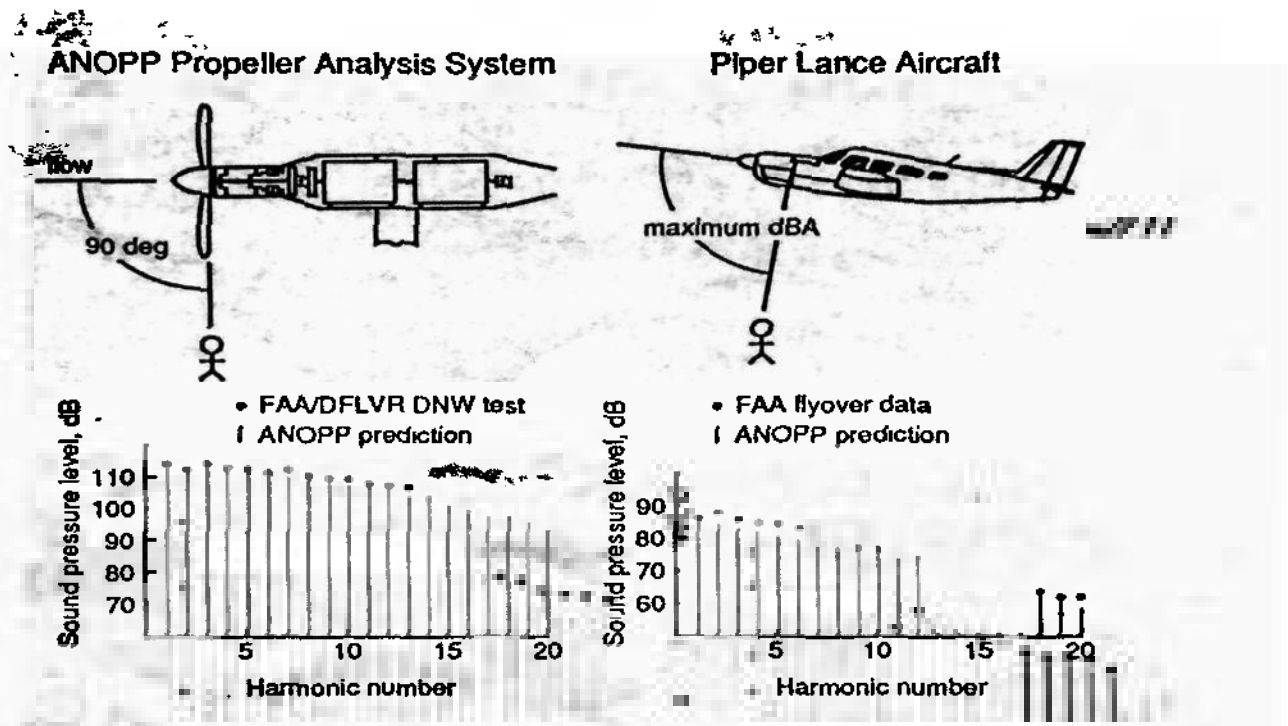


Figure 3.1.1 ANOPP-PAS Noise Predictions vs. Test Data [11]

To perform an ANOPP-PAS prediction, the user must define certain fundamental characteristics of the propeller and its operating environment. To execute the ANOPP program, the user develops an input file. This file contains all the geometric information needed to define the propeller as well as provides commands that enable ANOPP to perform all calculations, set parameter values,

Boolean operators, and the EXECUTE command that runs the individual sub-modules when all data parameters have been defined. When an analysis is initiated a script runs the input file, then the input file executes the sub-modules that define the propeller geometry, determine flight path, define an operating environment, calculate performance, and ultimately calculate the propellers noise characteristics. [5] The UNIX version of ANOPP-PAS is a very complex program that can be altered to provide very detailed performance and noise predictions.

In order to define the propeller geometry, the user enters the airfoil coordinates of a minimum of three spanwise stations as a function of propeller span in percent propeller radius. Additionally, ANOPP requires the definition of the leading edge abscissa and ordinate of the airfoil at each station, in real space normalized with respect to blade radius. The user also defines blade angle, chord length normalized with respect to the radius, leading edge radius normalized with respect to chord, and the number of upper and lower surface points that define each airfoil. It should be noted that all analysis performed in this research is executed with eleven spanwise stations defining the propeller geometry.

After the propeller geometry is defined, the user defines the number of blades, blade radius and the propeller rotational speed. The desired number of harmonics for near-field noise predictions is also specified. Then a table is generated to define the range of angles of attack and Mach numbers. This table

is used by ANOPP, through interpolation, to determine: lift, drag and many other quantities that help in the prediction of the propellers acoustic properties.

All aerodynamic characteristics of the propeller are predicted as a function of advance ratio. Therefore, thrust and power coefficients can be graphed as a function of advance ratio. Then the program is executed for the design cruise condition of 2400 rpm. Finally, the ANOPP-PAS program is run to provide performance and noise characteristics at the desired cruise condition. All far-field noise data in this analysis is predicted for steady level fly-over at 1000 ft. All near-field data is collected for the first 20 harmonics for varying polar directivity angles at 5R (five propeller tip radii).

ANOPP compares sound data in terms of OASPL, SPL, and A-weighted sound level. OASPL the overall sound pressure level adds most audible frequency components equally. SPL is equal to 20 times the logarithm to the base 10 of the ratio of the sound pressure to a reference pressure. A-weighted sound level is a sound pressure level that is weighted to approximate the response of the human ear by reducing the contributions of very low and very high frequencies. A-weighted sound pressure levels correlate closely with aircraft noise. [4]

4.0 Propeller Design

4.1 Design and Analysis

The design process of creating a quiet two bladed propeller began with the development of a two bladed reference propeller. The reference propeller was then utilized to examine the effects of varying design parameters on radiated noise and performance characteristics. Pre-determined propeller design criteria included the propeller diameter, range of rotational speeds and the cruise speed. Airfoils, lift coefficients, blade chord and twist distributions all had to be selected in order to define the basic reference propeller design. In order to avoid noise creating shock waves at the propeller tip, the rotational speed was selected to be 2400 RPM, which is typical of small aircraft rotational speeds during cruise. To prevent stalling the propeller at low advance ratios, it is necessary that the airfoils exhibit good trailing stall characteristics at large angles of attack.

4.2 Reference Propeller Definition

The first step in defining the reference propeller required definition of the propeller airfoils. Several series were examined including: NACA 44XX, 66XX, 16XX and the Clark-Y airfoil series. These series were all selected based on maximum lift coefficient, trailing edge stall characteristics, and angle of zero lift. Trial reference blade cases were established for each series with the thinnest airfoils located at the tip increasing to the thickest sections at the propeller's root. Initial testing with ANOPP's performance module indicates that the NACA 44XX series is best for the reference propeller because it demonstrates superior power and thrust performance due to high $C_{l_{max}}$ and smooth trailing edge stall characteristics.

There are three desirable characteristics required in selection of a blade shape for a fixed pitch propeller. They are; smooth pressure distribution, large maximum sectional lift coefficient $C_{l_{max}}$, and good trailing edge stall characteristics. The propeller advance ratio J is defined by the relation,

$$J = V_0/nD \qquad \text{Equation 2.1.1}$$

where V_0 is the free-stream speed, n is the propeller rotational speed in rev/sec and D is the propeller diameter [6]. At zero advance ratio, i.e. when V_0 is zero, the propeller is typically in a highly stalled condition at inner radial stations. This fact requires that the airfoil shape have a large $C_{l_{max}}$ to achieve large thrust levels and significant C_l at angles of attack (α) larger than where $C_{l_{max}}$ occurs. These stall characteristics are indicative of trailing edge stall. The NACA 44XX series of

airfoils exhibit these desirable trailing edge stall characteristics as can be observed in Figure 4.2.1, where experimentally obtained sectional lift coefficient is plotted as a function of α for a NACA 4412 airfoil. [19]

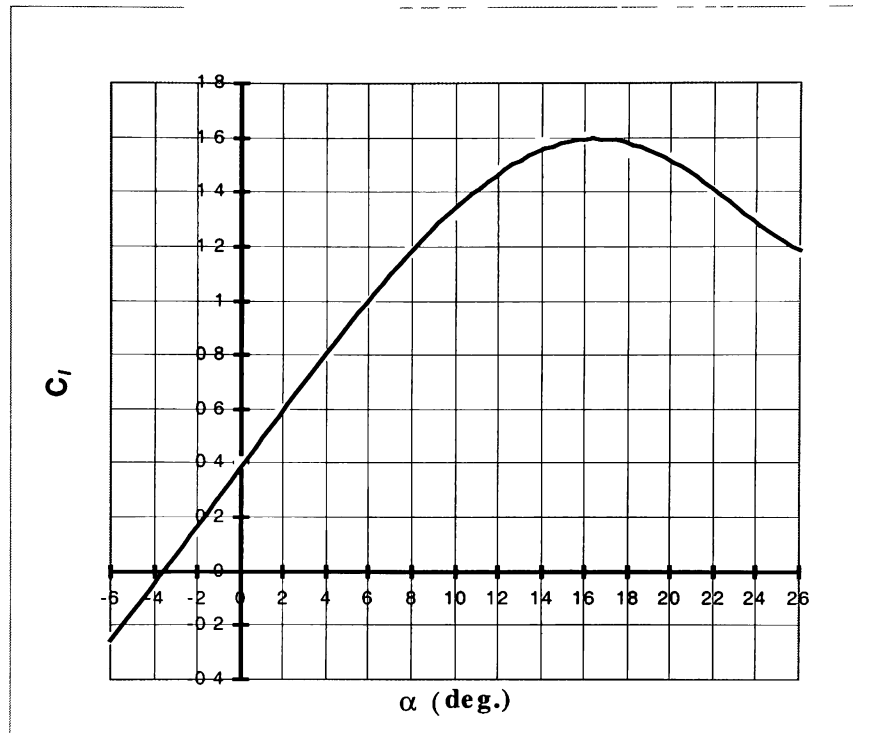
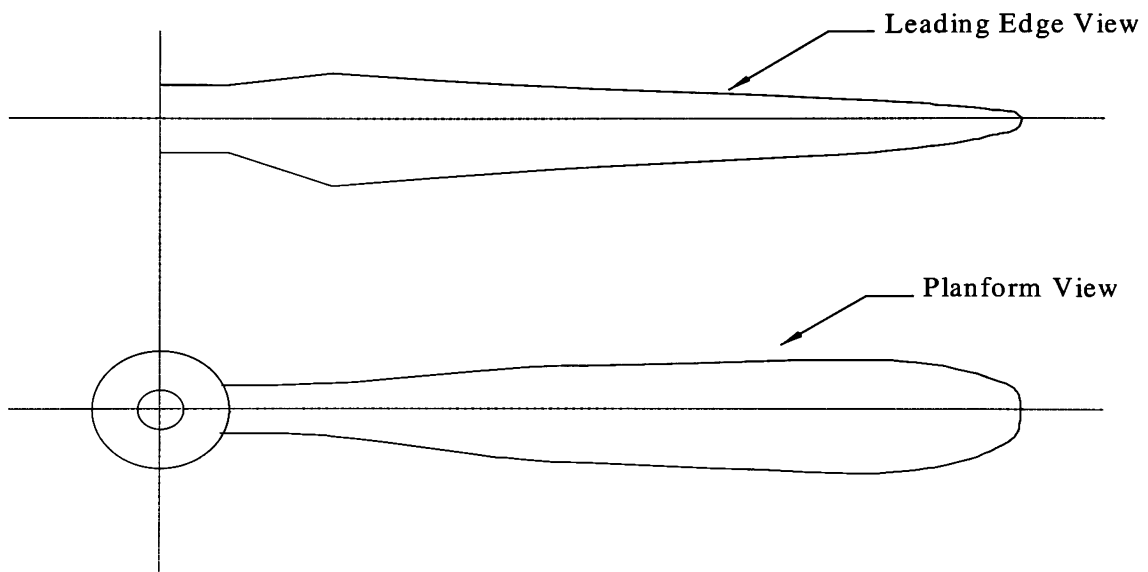


Figure 4.2.1 NACA 4412 Sectional lift coefficient C_l vs. angle of attack α .

At an advance ratio J of zero and r/R of 0.5 the reference blade has an α of 24.8° , inspection of Figure 4.2.1, indicates a sectional lift coefficient of 1.25. The 44XX airfoil series also exhibits smooth pressure distributions at small α which results in a smooth distribution of radiated noise tones at blade-passing-frequency (BPF) and harmonics. [20] The NACA 4412 has a high C_{lmax} of 1.6 compared to the Clark-Y with C_{lmax} of 1.4. [21] Inspection of Figure 4.2.1, also reveals that at α greater than 17° the sectional lift coefficient falls off gradually

this characteristic is indicative of an airfoil with good trailing edge stall characteristics.

Presented in Figure 4.2.2 is a top view sketch of the blade plan-form shape of the reference blade as well as a leading edge view.



Blade6.5-44s

Figure 4.2.2 Sketch of the reference propeller blade.

Table 4.2.1 illustrates the fundamental design properties of the reference propeller. Starting with the distribution of airfoil sections for the propeller as a function of radial position r/R where r is the radial position measured from the

center of rotation and R is the blade tip radius, which is taken to be 38 inches. The reference propeller is thus, a two-bladed propeller with a tip diameter of 76 inches. The other design criteria are a free-stream speed of 160 kts and a propeller rotational speed of 2,400 rpm, resulting in a design advance ratio J of 1.07. These characteristics are typical of GA propellers such as the Hartzell model F8475D-4. Also shown in table 4.2.1 are the blade chord c, blade angle β and sectional lift coefficient C_l as a function of r/R. Inspection of this table shows that the NACA 4406 airfoil is used at the tip and the airfoil thickness increases as r/R decreases until the NACA 4418 airfoil is used at a r/R of 0.2. It is assumed that the spinner radius will be located at r/R of 0.2. The blade tip has an elliptical shape starting at r/R of 0.8, i.e. the outer 7.6 in. of the blade tip. The solidity of the reference propeller is $\sigma = .092$ and the Activity Factor $AF = 112$ both of which are typical for two bladed fixed pitch propellers. [22]

Table 4.2.1 Helix, Blade and Attack angles, chord c, and Sectional Lift Coefficient C_l as a Function of Radial Position r/R at a Design Advance Ratio of 1.07.

NACA AIRFOIL	r/R	r	ϕ	α_i	ϕ_s	β	α	c	C_l
4418	0.20	7.60	59.48	27.79	87.27	65.03	37.24	6.50	0.75
4415	0.30	11.40	48.51	21.04	69.55	53.05	32.01	6.50	0.75
4415	0.40	15.20	40.30	16.96	57.26	44.70	27.74	6.50	0.75
4412	0.50	19.00	34.16	13.68	47.84	38.49	24.81	6.50	0.75
4412	0.60	22.80	29.48	12.21	41.69	33.77	21.56	6.50	0.75
4412	0.70	26.60	25.86	10.72	36.58	30.11	19.39	6.50	0.75
4412	0.75	28.50	24.34	9.98	34.32	27.98	18.00	6.50	0.70
4412	0.80	30.40	22.98	9.31	32.29	26.01	16.70	6.50	0.65
4409	0.85	32.30	21.76	8.56	30.32	23.58	15.02	6.31	0.58
4409	0.90	34.20	20.65	8.00	28.65	21.87	13.87	5.72	0.45
4409	0.95	36.10	19.65	7.47	27.12	20.26	12.79	4.55	0.42
4406	0.975	37.05	19.19	7.16	26.34	19.19	12.04	3.59	0.40
4406	0.995	37.81	18.83	7.02	25.84	18.83	11.81	2.41	0.40
4406	1.00	38.00	18.74	6.98	25.72	18.74	11.76	1.98	0.40

Additionally the blade, effective helix angle Φ_e , blade helix angle Φ , and the lift induced angle of attack α_i are included in Table 4.2.1 and all are defined below in Equations 4.2.2- 4.2.5. [20] A sketch representing the various angles is shown in Figure 2.1.3.

$$\beta = \Phi_e + \alpha \quad \text{Equation 4.2.2}$$

$$\Phi_e = \Phi + \alpha_i \quad \text{Equation 4.2.3}$$

$$\Phi = \tan^{-1} (V_o / V_t) \quad \text{Equation 4.2.4}$$

$$\text{Equation 4.2.5}$$

$$\alpha_i = - \left[- \left[\frac{1}{x} + \frac{\sigma \cdot V_R}{8x^2 \cdot V_T} \right] + \left[\left(\frac{1}{x} + \frac{\sigma \cdot V_R}{8x^2 \cdot V_T} \right)^2 + \frac{\sigma \cdot V_R}{2x^2 \cdot V_T} \cdot (\beta - \phi) \right]^{1/2} \right]$$

Using the propeller rotational speed and free-stream velocity, the helix angle is calculated using equation 4.2.4. V_o and V_t represent the free stream speed and tangential component of the rotational speed respectively. The design lift coefficient determines the angle of attack for each respective airfoil section. The blade angle β is calculated through the following iterative process: first an initial blade angle is selected and assumed to be the sum of the helix angle and the

angle of attack, then with the value of β the induced angle of attack is derived using Equation 4.2.5 and in turn the helix inflow angle is calculated. Used in Equation 4.2.5 is the advance ratio J , the lift curve slope is a , V_R and V_T are the resultant velocity and tangential component of the velocity respectively, and the blade solidity σ is the ratio of total blade area to propeller disk area. The iterative process is repeated until the blade angle is nearly constant from iteration to iteration i.e the blade angle is changing by less than a hundredth of a degree for each iteration. Figure 4.2.3 represents the blade angle distribution β as a function of r/R , for the reference propeller.

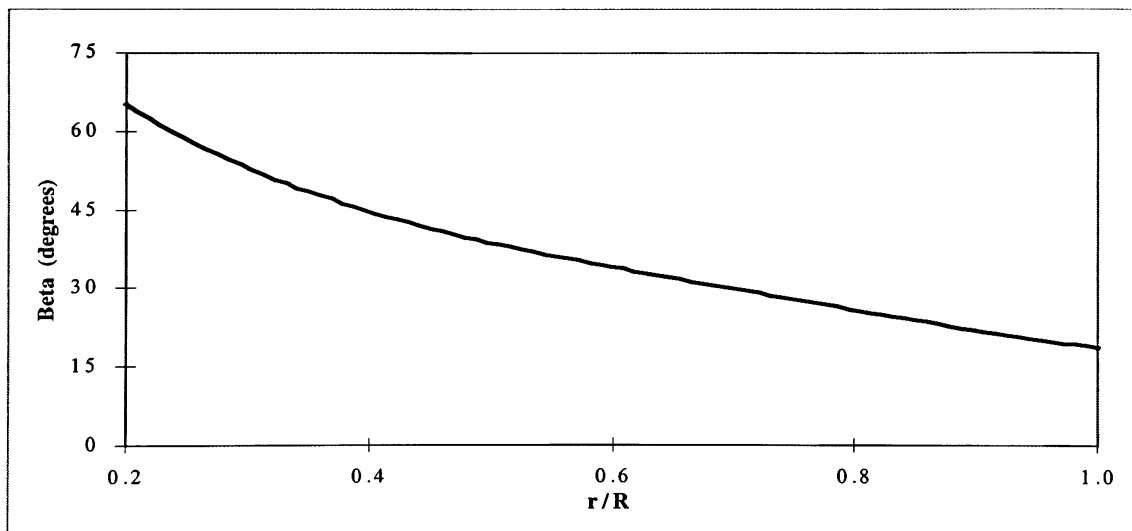


Figure 4.2.3 Reference propeller Beta vs. r/R

Propeller weight is a significant issue in GA aircraft; to ensure that the reference propeller is reasonably well designed with respect to weight, the propeller volume is calculated. The hub volume is based upon a hollowed right circular cylinder; the top view of the hub is illustrated in Figure 4.2.2. The hub is integrated with the blade at r/R of 0.2; additionally the hub is 6 in. diameter, and

3.25 in. thick. This hub has a 2.25 in. diameter hole at the centerline and 6 mounting holes of 0.5 in. diameter equally spaced on a 4.5 in. bolt circle diameter. Based upon these criteria, the volume for the 2-bladed reference propeller is 296 in³ which is equivalent to approximately 30 lb. for the propeller fabricated from solid forged aluminum. The reference blade weight compares to 35 lb. for a solid aluminum Sensenich propeller of 74 in. diameter used for the Piper Cherokee 165 and is thus reasonably designed with respect to weight.

4.3 Reference Propeller Aerodynamic Performance (NACA Airfoils)

Shown in Figure 4.3.1 are the reference propeller aerodynamic performance characteristics, where the thrust coefficient C_T , power coefficient C_P , and efficiency η are plotted as a function of advance ratio J . The C_T , C_P , and η parameters are given by the following relationships.

$$C_T = T/\rho n^2 D^4 \quad \text{Equation 4.3.1}$$

$$C_P = P/\rho n^3 D^5 \quad \text{Equation 4.3.2}$$

$$\eta = (C_T/C_P)J \quad \text{Equation 4.3.3}$$

The design is based on a free-stream speed of 160 kts, blade tip diameter D of 76 inches, and propeller rotational speed n of 2,400 rpm, which in turn results in a design advance ratio J of 1.07 at level cruise conditions. At

the design J of 1.07, C_T is 0.0447, C_P is 0.0542, and η is 87.9%. These aerodynamic performance coefficients, at standard sea-level conditions, result in a thrust of 260 lb and power of 145 hp which gives a thrust to power ratio (T/P) of 1.79 lb./hp. Limitations in programming format cause compounded extrapolation errors which result in non-exact performance parameters at $J < 0.55$. Therefore below $J = 0.55$ the performance curves can only be used for general tendencies, and not for performance parameters[5]. For the airfoils selected, good take off performance will be assured as long as C_T is above 0.07 at zero advance ratio. The specified power of 145.0 hp actually constitutes the required power for level flight which is based on approximately 70% of the assumed available power of about 200 hp. The excess power is necessary for the aircraft to climb and maneuver.

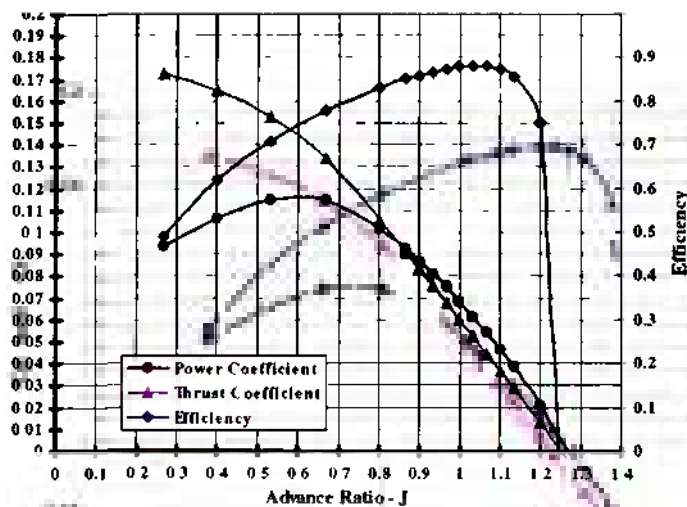


Figure 4.3.1 Aerodynamic Performance Characteristics for the Reference Propeller (NACA Airfoils).

The predicted reference propeller aerodynamic performance parameters compare favorably with published propeller data and thus, it is evident that the design is more than adequate for GA aircraft [6,9,10]. Therefore the reference propeller will function as well or better, than presently manufactured GA aircraft propellers.

4.4 Radiated Noise Characteristics of Reference Propeller

Presented in Figure 4.4.1 is the predicted unweighted near-field OASPL plotted as a function of directivity angle. The directivity angle is measured from directly in front of the propeller in a vertical plane, i.e. directly ahead is zero degrees, in the plane of propeller rotation is 90° and directly behind is 180° as shown in Figure 4.4.2. All near-field noise predictions reported are located in a vertical plane at a distance of 5R (five propeller tip radii) of the propeller center of rotation. A distance of 5R is 15.8 ft which is equivalent to 1.13 of a wave length at standard sea-level conditions and a blade-passage-frequency (BPF) of 80 Hz. Inspection of this curve indicates that the maximum near-field OASPL of 111.2 dB occurs at a directivity angle of 105° . At 105° the equivalent maximum A-weighted OASPL is 96.4 dBA.

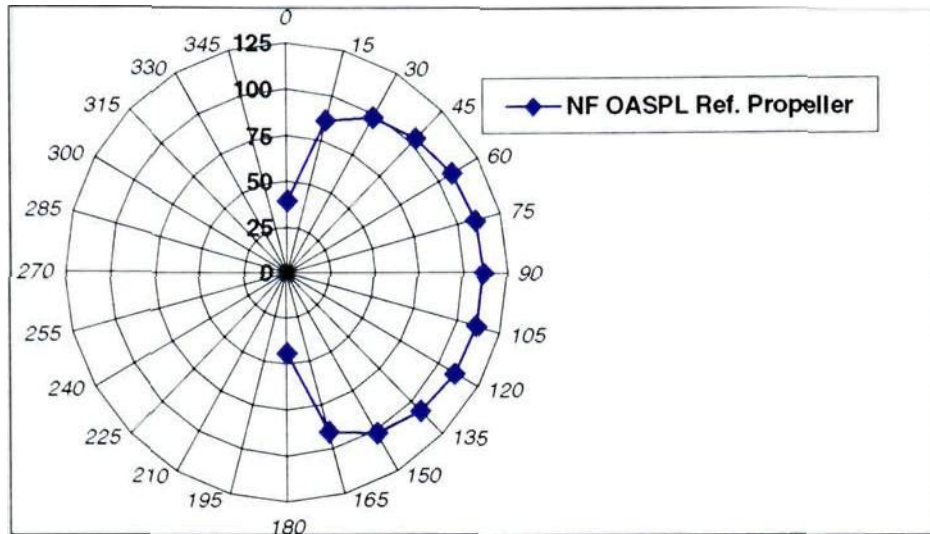


Figure 4.4.1 The Near-Field OASPL (dB) Re: 20 μ Pa as a Function of Directivity Angle.

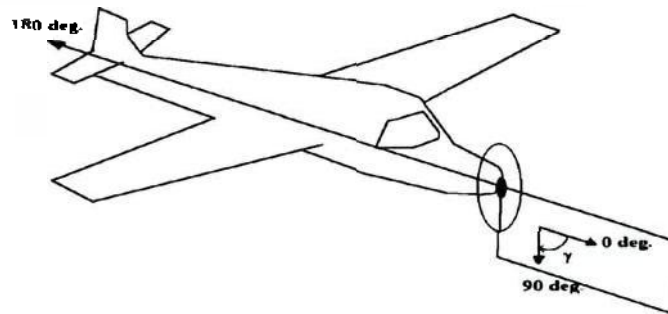


Figure 4.4.2 Sketch of Directivity Angle γ .

Presented in Figure 4.4.3 is the near-field sound-pressure-level (SPL), thickness and loading noise plotted as a function of harmonic number for the same prediction case as presented in Figure 4.4.1, at a directivity angle of 105°. This figure constitutes the frequency spectrum where the harmonic number indicates the integer times BPF, e.g. a harmonic number of three constitutes the tone at three times BPF, thus if BPF=80 Hz then 3BPF= 240 Hz. Examination of the curve reveals a monotonic decrease in the magnitude of the tones with the maximum occurring at BPF which is indicative of a smooth blade pressure

distribution. [10] Table 4.4.1 illustrates the contributions of the thickness noise and the loading noise, both of which are listed as a function of harmonic number and tonal frequency, for the same near-field case as presented in Figure 4.4.1. The table shows that the loading noise dominates thickness noise at BPF and 2BPF, are essentially equal at 3BPF and at tones of 4BPF and greater, that thickness noise dominates. This information indicates that the unweighted OASPL is dominated by blade loading noise, but that the A-weighted OASPL is dominated by thickness noise. This phenomenon occurs because the A-weighting function greatly attenuates the low frequency tones, e.g. at BPF the actual SPL is reduced by 22.5 dB. The reason that the sum of the loading and thickness noise are less than might be expected is due to the difference in phase angle of the two additive components.

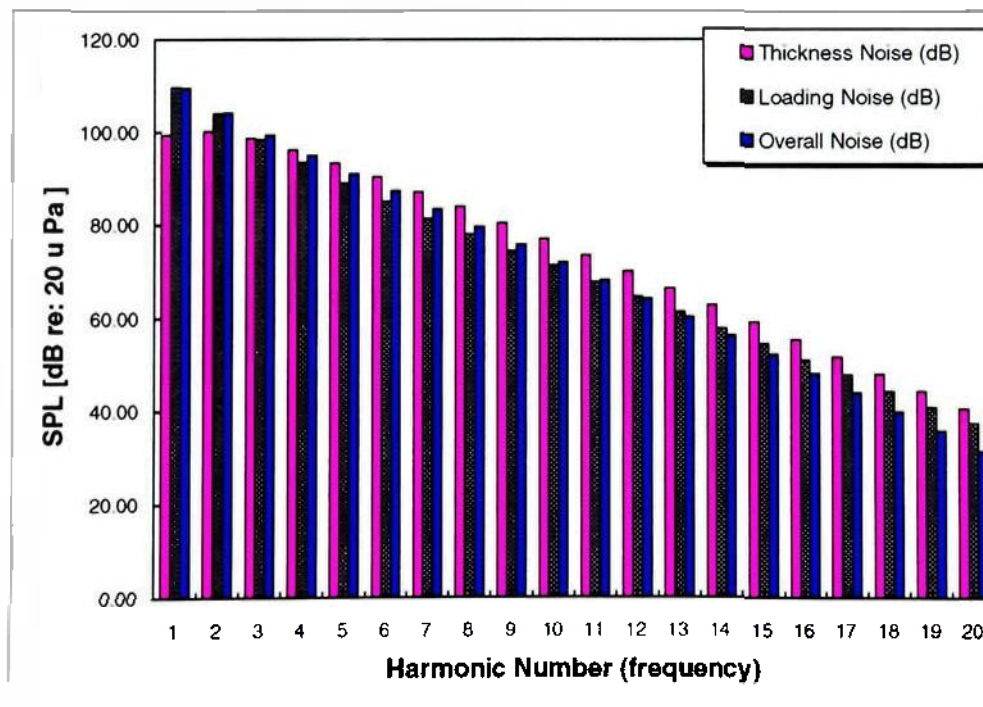


Figure 4.4.3 SPL Frequency Spectrum of the Near-Field Noise in Terms of Harmonic Number for the Reference Propeller.

Table 4.4.1 Reference Propeller Near-field Thickness and Loading Noise as a Function of Harmonic Number at Directivity Angle 105°.

OASPL = 111.2

Harmonic Number	Frequency (Hz)	Thickness Noise (dB)	Loading Noise (dB)	Overall Noise (dB)
1	80	99.28	109.68	109.54
2	160	100.14	103.91	104.18
3	240	98.59	98.43	99.39
4	320	96.20	93.47	95.10
5	400	93.39	89.02	91.09
6	280	90.32	85.01	87.21
7	560	87.10	81.31	83.38
8	640	83.77	77.81	79.56
9	720	80.36	74.41	75.72
10	800	76.90	71.06	71.86
11	880	73.38	67.74	67.99
12	960	69.83	64.41	64.07
13	1040	66.24	61.07	60.12
14	1120	62.63	57.73	56.14
15	1200	58.99	54.36	52.11
16	1280	55.32	50.98	48.05
17	1360	51.64	47.76	43.94
18	1440	47.93	44.18	39.80
19	1520	44.21	40.75	35.60
20	1600	40.46	37.30	31.34

Shown in Figure 4.4.4 is the far-field unweighted over-all-sound-pressure-level (OASPL) in decibels, with respect to $20 \mu\text{Pa}$, predicted at ground level with the aircraft flying overhead in level flight at an altitude of 1000 ft, for the reference propeller. This noise prediction is with the microphone placed 1.2 meters above the ground, at the origin of the reference frame. The maximum predicted unweighted OASPL of 76.9 dB shown in this curve is equivalent to an A-weighted level of 65.9 dBA. Due to the directivity characteristics of the radiated noise of propellers, the maximum OASPL occurs almost one second after the aircraft has passed the nearest point of approach. The maximum radiated propeller noise occurs slightly behind the propeller plane of rotation as expected. [12]

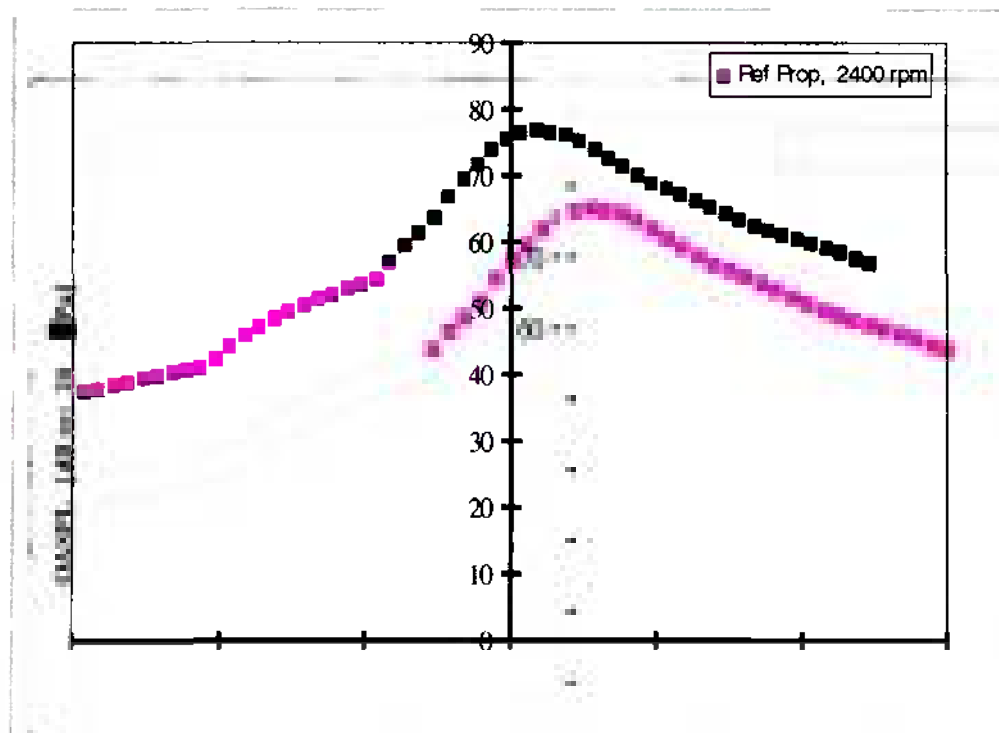


Figure 4.4.4 Far-field Radiated Noise at 1000 ft. (OASPL vs. time) for the Reference Propeller @ 2400 RPM

4.5 Effects of Tip Shape on Radiated Noise Characteristics

The use of an elliptical tip shape in the reference propeller design is based upon a study where the reference propeller tip shape is varied, the radiated noise characteristics are predicted and the results compared. Four cases are studied, the nominal thrust of 260 lb and the nominal power of 145 hp, are maintained within a couple of percent of one another. For the elliptical tip, the ellipse is faired into the blade such that maximum thickness is located where the blade chord is 6.5 in. and 7.6 in. from the blade tip. The blade chord is zero at the tip for the elliptical tipped blade. In a similar manner, a parabolic tip is analyzed. The third case is a circular tip where the radius is half the chord of 6.5 in. with the blade chord being zero at the tip. The fourth case is a square tip where the 6.5 in. blade chord remains the same all of the way to the blade tip.

Table 4.5.1 illustrates the maximum unweighted and A-weighted OASPL in the Far-Field for 1000 ft in level flight, and the near-field at 105° directivity angle, for the various blade tip shapes considered in the investigation. This blade tip evaluation is with the 2-bladed reference propeller, 76 in. diameter, rotating at 2400 rpm in a free-stream flow field of 160 kts. Inspection of this table shows that

the near-field unweighted OASPL for all tip configurations are all around 111 dB with minor variation.

Table 4.5.1 Unweighted and A-weighted OASPL, Maximum Far-Field and Near-Field Levels at a Directivity Angle of 105°, for Different Propeller Tip Shapes.

Max	Square	Circular	Parabolic	Elliptical
Near-Field (dB)	111.1	111.1	110.6	110.9
Far- Field (dB)	84.5	84.5	83.5	84.0
Far Field (dBA)	72.3	73.9	69.9	73.5

Table 4.5.1 also shows that the unweighted far-field OASPL for the square and circular tips are 84.5 dB and the OASPL for the parabolic and elliptical tips are respectively 1.0 dB and 0.5 dB less. For the A-weighted far-field OASPL, the circular tip is the noisiest at 73.9 dBA and the levels for the elliptical, square and parabolic tips are respectively 0.4 dBA, 1.6 dBA, and 2.4 dBA less.

Again, the difference between the unweighted and A-weighted OASPL is due to the thickness and loading noise frequency distributions. In three of the four noise categories, the parabolic tip resulted in the lowest noise levels and the elliptical tip resulted in the second quietest configuration. Due to these noise characteristics, the final selection of the tip shape was narrowed down to the parabolic and elliptical tip shapes. The A-weighted noise considerations show that the parabolic tip shape results in significant noise reduction with respect to the circular tip design. However, the parabolic blade was eliminated from consideration due to its design transition characteristics i.e. the intersection of the

parabolic tip distribution and the constant blade chord results in a sharp corner on the blade. High stress concentrations at the sharp corner, inherent problems in manufacturing and human factors all force the parabolic design to be eliminated from consideration. Therefore, the elliptical tip shape was chosen for the reference blade as it is best configuration based upon noise, human factors and manufacturing considerations.

4.6 Propeller Rotational Speed

Single engine aircraft operate at cruise in a range of 2400 to 2500 rpm and as high as 2700 rpm during take-off and at other times when the engine is run-up to full power. Because the propeller is designed with noise characteristics in mind, the reference propeller is optimized for the lower end of the rotational spectrum at 2400 rpm. Using full power the reference propeller is rotated at 2700 rpm, and the propeller advance ratio decreases from 1.07 to 0.95. Referring to Figure 4.3.1, the propeller aerodynamic performance curves indicate that the new advance ratio J will result in aerodynamic performance characteristics where C_P is 0.075, C_T is 0.0679 and an efficiency of 87.0%. These quantities at standard sea level result in a thrust of 394 lb. and power of 200 hp, which gives a thrust to power ratio of 1.96 lb/hp where 200 hp will normally constitute the maximum power available for the aircraft considered.

Rotating a 76 in diameter propeller at 2700 rpm while generating lift at the tip will always result in shock waves being formed which, of course, generates a considerable amount of noise. The airfoils near the tip for the reference propeller

are designed to have a sectional lift coefficient of 0.40, as can be seen by reviewing Table 4.2 1, while rotating at 2,400 rpm. At these conditions, a study of the pressure distribution reveals that the peak flow velocity near the tip is 0.92M and, therefore, no shock waves will form on the blade tip at 2400 rpm.

Shown in Figure 4.6.1, is the far-field OASPL radiated noise characteristics of the reference propeller rotating at 2400 rpm and 2700 rpm. Examination of these curves indicates that at 2700 rpm, the OASPL is higher than at 2400 rpm by approximately 6 dB during approach and 9.5 dB greater at the peak level as well as during the departure. Interestingly, the noise is estimated to be 3 dB to 10 dB greater than predicted because the ANOPP-PAS program predicts the noise associated with the shock wave interaction with the blade but not the direct radiation from the shock or from the shock oscillation.

[20]

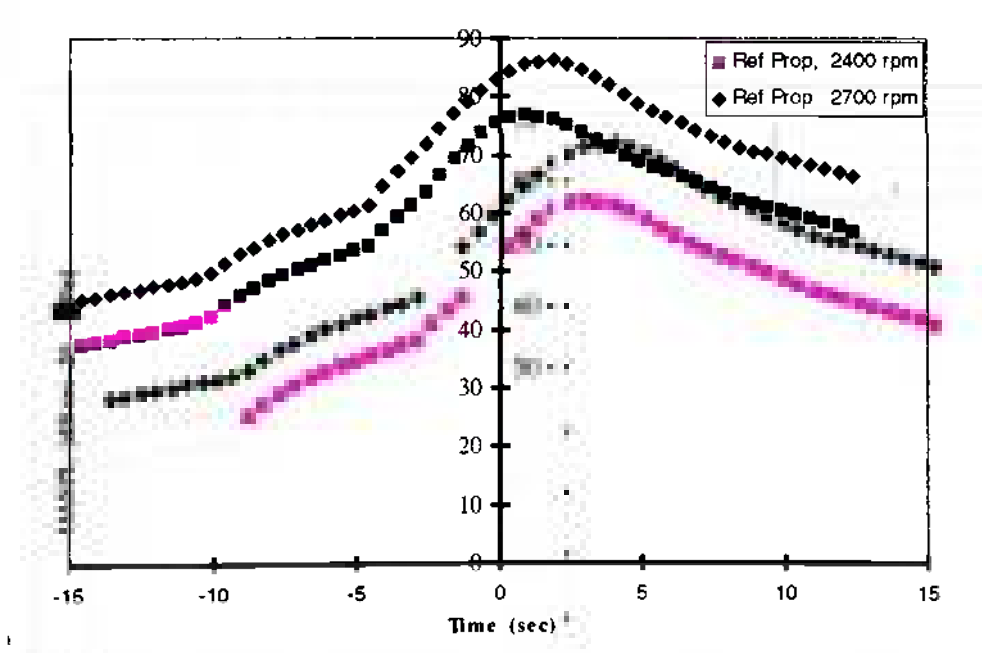


Figure 4.6.1 Far-Field OASPL Radiated Noise Characteristics of Reference Propeller Rotating at 2,400 rpm, and 2,700 rpm.

Presented in Figure 4.6.2 is the predicted frequency distribution of the near-field SPL for the reference propeller rotating at 2400 rpm and 2700 rpm, both at a directivity angle of 105°. It is important to note that BPF at 2400 rpm is 80 Hz and at 2700 rpm BPF is 90Hz, hereafter referred to as BPF_{lo} and BPF_{hi} respectively. Review of this figure reveals that at the first tone that BPF_{hi} is approximately 8 dB greater than BPF_{lo} and the decibel difference steadily increases to the highest harmonic tone at $20BPF_{hi}$ (1,600 Hz) which is approximately 34 dB greater than $20BPF_{lo}$ (1,800 Hz). For the data shown in Figure 4.6.2, the unweighted OASPL is 111.2 dB at 2400 rpm and is 9.6 dB greater at 2700 rpm, while the A-weighted OASPL is 96.4 dBA at 2400 rpm and is 14.0 dBA greater at 2700 rpm.

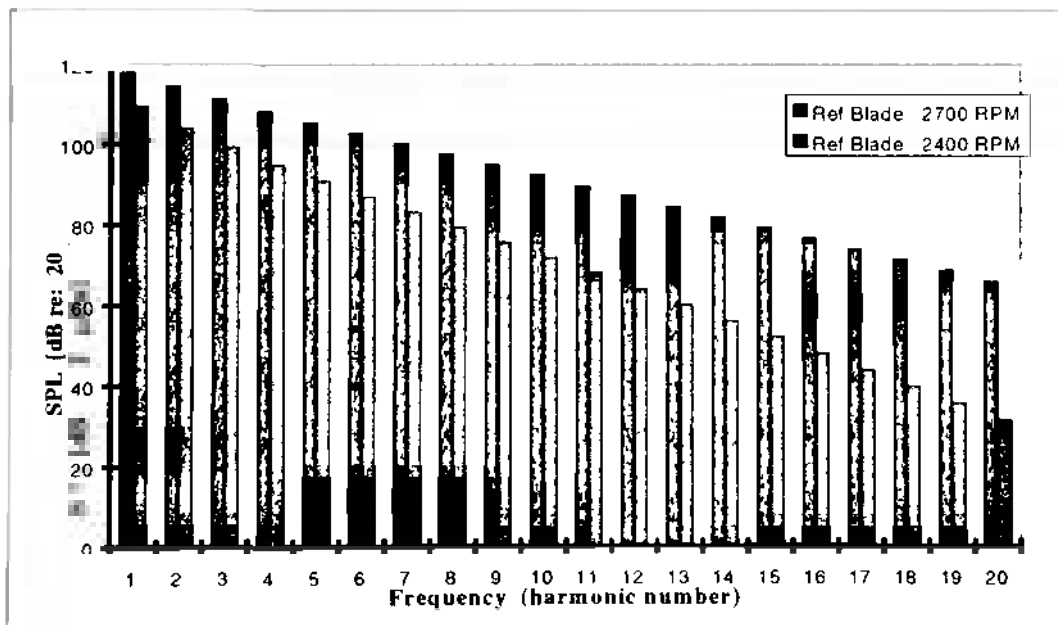


Figure 4.6.2 Frequency Distribution of Near-Field SPL of the Reference Propeller Rotating at 2400 and 2700 rpm, both at 105° Directivity Angle.

The shock wave formation at 2700 rpm, creates considerably more noise at the higher harmonics than at the lower ones and has a greater affect on the A-weighted level than for the unweighted case. Moreover, the effect of shock wave formation will result in a greater increase in the A-weighted level than in the unweighted level. Again it is important to note that ANOPP-PAS contains a known under-prediction of shock wave noise of 3-10dB [20].

This comparison demonstrates that in order to reduce noise radiated from large diameter propellers it is necessary to prevent shock waves from forming at the tip. To prevent excess noise generation 76 in. diameter propellers should be designed for optimal cruise rotational speeds less than approximately 2400 rpm. Clearly the reference propeller is designed to meet this low noise criteria by avoiding tip shock waves during aircraft operations. The most severe noise case occurs during climb when the maximum engine power and rotational speed are encountered. To satisfy environmental noise considerations, it is very important that blade tip shock waves not be generated.

4.7 Effects of In-Plane Sweep

The use of sweep in propeller design has been well established as a means of reducing radiated noise of propellers. Swept propeller designs can reduce propeller noise using both in-plane and out-of-plane sweep [4,17]. The basic concept is that the noise source is distributed over the propeller blade surface [12,13] and that there can be noise cancellation at a point away from the propeller due to acoustic pressure wave cancellation. [25,26] The scimitar

shaped blades used on the ultra-high bypass prop-fan are designed based upon this concept using both in-plane and out-of-plane sweep. [4]

For in-plane sweep, three basic sweep configurations are considered all of which are developed from the reference propeller, i.e. the 2-bladed configuration previously discussed. Sweep is incorporated into the reference propeller design by creating an ellipse and then forcing the leading edge of the reference propeller to follow one quarter of its elliptical arc in the plane of the propeller. The trailing edge is then defined from the new leading edge with equivalent chords from the reference propeller. This method transforms the elliptical tip shape such that the leading edge is drastically elongated and the trailing edge is slightly elongated and straightened. The degree of change due to sweep of the reference blade is then dependent on the chosen sweeping ellipse and the location of where it is incorporated into the design. The first configuration considered is based upon the sweep starting at the 0.2 r/R position sweeping aft in the plane of rotation and is called full sweep, with the designation IPSE following by a number designating the amount of sweep displacement at the tip in inches, e.g. IPSE-3 means 3 inches of tip sweep. The IPSE configurations are evaluated with 3 in., 6.5 in. and 13 in. of tip sweep. The second basic configuration consists of the aft in-plane sweep starting at 0.5 r/R position and designated as HIPSE with an ultimate tip sweep of 6.5 in. only. The third configuration consists of in-plane aft sweep starting at the 0.75r/R position which is designated as QIPS with tip sweep of 6.5 in. and 9.75 inches. Shown in Figure 4.7.1 are the planform views for all of the

swept configurations discussed, the figures are labeled with the appropriate configuration designation. There are many other swept configurations that can be evaluated including combination configurations with forward sweep near the hub and aft sweep near the tip [17] as well as blades with out-of-plane sweep [4] which is discussed in section 4.8.

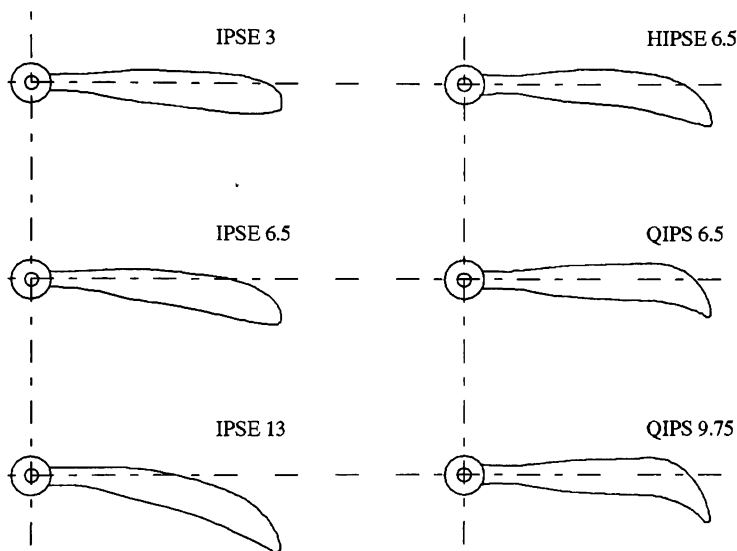


Figure 4.7.1 Planform View of all In-plane Swept Blade Configurations.

The far-field fly-by OASPL as well as the near-field OASPL and SPL frequency spectrum noise levels are evaluated for all swept configurations and the thrust and power at cruise conditions are all within 2% of the reference propeller. Shown in Figure 4.7.2 is the unweighted far-field OASPL at fly-over during level flight at 1000 ft altitude for the HIPSE-6.5 configuration as well as the reference propeller. Comparing the two OASPL curves indicates that the swept blade is 1.0 dB quieter than the upswept case during approach and at the peak levels, while during departure very little difference is seen in the OASPL.

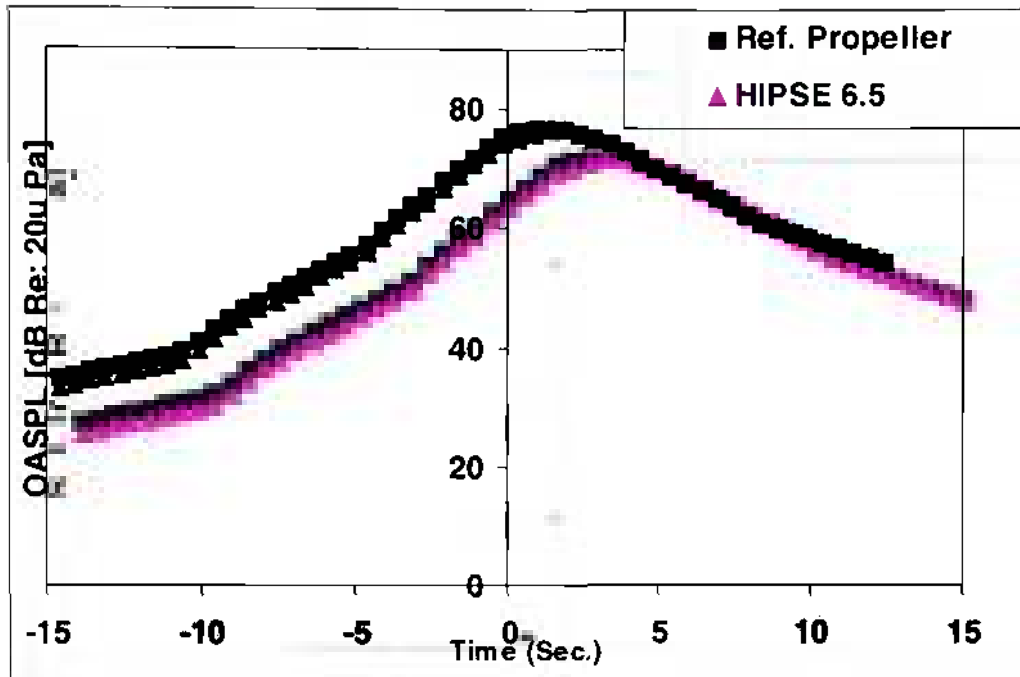


Figure 4.7.2 Far-field OASPL at 1000 ft for HIPSE 6.5 and the Reference Propeller.

Shown in Table 4.7.1 is the maximum far and near field OASPL for all in-plane sweep configurations including the reference propeller data for comparison. The maximum peak far-field non-weighted and A-weighted OASPL is predicted during fly-over at a 1000 ft altitude and the near-field OASPL is at a 105° directivity angle. Inspection of this Table reveals that in-plane sweep does reduce both the far-field and near-field non-weighted and A-weighted OASPL. The HIPSE-6.5 and QIPS-9.75 swept configurations exhibit the lowest noise levels relative to the reference propeller. For example relative to the reference

propeller, the HIPSE- 6.5 in the far-field is 0.6 dB and 2.2 dBA quieter, and in the near-field is 0.5 dB and 1.4 dBA quieter.

Table 4.7.1 Maximum Non-Weighted and A-Weighted OASPL, Near and Far-Field, for all Blade Configurations.

	Reference Propeller	IPSE 3	IPSE 6.5	IPSE 13	QIPS 6.5	QIPS 9.75	HIPSE 6.5
Far OASPL (dB)	76.9	76.6	76.3	76.0	76.0	75.5	76.3
Far OASPL (dBA)	65.9	65.5	65.2	65.0	64.6	64.0	63.7
Near OASPL (dB)	111.2	111.0	110.9	111.0	110.7	110.4	110.7
Near OASPL (dBA)	96.4	96.0	95.6	95.4	95.0	94.3	95.0

For the cases considered the tables show, the greater the in-plane sweep the lower the noise as expected [27]. Based upon these predictions, the HIPSE-6.5 configuration is recommended because it exhibits superior noise reduction characteristics, it is significantly quieter in the far- and near-fields especially in the A-weighted case than the reference case. The half-swept with 6.5 in. of tip sweep (HIPSE-6.5) configuration is also easier to manufacture than the full-swept (IPSE) and quarter-swept (QIPS) configurations.

4.8 Effects of Out-of-Plane Sweep

As discussed previously the use of sweep in propeller design is well established as a means of reducing radiated noise of propellers. As with in-plane sweep, the basic concept is that the noise source is distributed over the propeller blade source [12,13] and that there can be noise cancellation at a point away from the propeller because of acoustic pressure wave cancellation. [25,26]

Two out-of plane configurations are swept in a similar manner to the in-plane designs. Sweep is incorporated into the reference propeller design by creating an ellipse and then forcing the leading edge of the reference propeller to follow one quarter of its elliptical arc aft of the propellers plane of rotation. The trailing edge is then defined from the new leading edge with equivalent chords from the reference propeller. The degree of change due to sweep of the reference blade is then dependent on the chosen sweeping ellipse and the location of where it is incorporated into the design. The first configuration is based upon the sweep, starting at the 0.2 r/R position sweeping aft in the plane of rotation. This configuration is called full out-of-plane sweep, with the designation OPSE following by a number designating the amount of sweep displacement at the tip in inches, e.g. OPSE-1.3 means 1.3 inches of tip sweep. The OPSE configurations are evaluated with 1.3in., 2.6 in., 3.9 in., and 6.5 in. of tip sweep. The second configuration consists of the aft out-of-plane sweep starting at 0.5 r/R position and designated as HOPSE with the same amount of tip sweep as the first configurations.

The far-field fly-by OASPL as well as the near-field OASPL and SPL frequency spectrum noise levels are evaluated for all swept configurations and the thrust and power at cruise conditions are all within 1.5% of the reference propeller. Figure 4.8.1 illustrates the non-weighted far-field OASPL at fly-over during level flight at 1000 ft altitude for the OPSE-6.5 configuration and the reference propeller. Comparing the two OASPL curves in the figure indicates that the blade swept out of plane is 1.8 dB quieter than the non-swept case 10 seconds prior to reaching the observer and 1.5 dB quieter just past the observer (peak); departure OASPL values are nearly identical. As with the reference propeller, OPSE6.5 has a maximum Near-Field OASPL at a directivity angle of 105°.

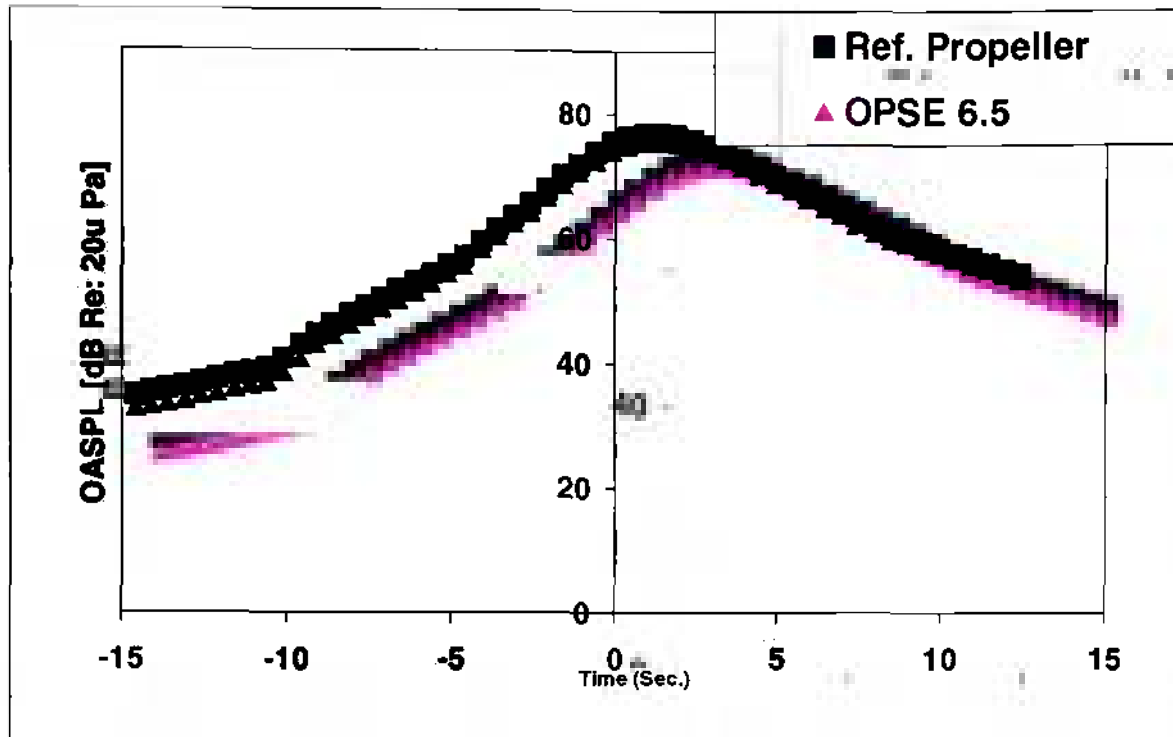


Figure 4.8.1 Far-field OASPL at 1000 ft for OPSE 6.5 and the Reference Propeller

Table 4.8.1 contains the maximum far and near field OASPL for all out-of-plane sweep configurations including the reference propeller data for comparison. Inspection of this Table reveals that out-of-plane sweep does reduce both the far-field and near-field unweighted and A-weighted OASPL. The OPSE-6.5 configuration exhibits the lowest noise levels relative to the reference propeller. For example relative to the reference propeller, the OPSE-6.5 in the far-field is 1.8 dB and 1.4 dBA quieter, and in the near-field is 3 dB and 2.5 dBA quieter.

Table 4.8.1 Maximum Far and Near Field OASPL for all Out-of-plane Swept Configurations

	Reference Propeller	OPSE-1.3	OPSE-2.6	OPSE-3.9	OPSE-6.5
Far OASPL (dB)	76.9	76.3	76.1	75.6	75.1
Far OASPL (dBA)	65.9	66.4	66.2	65.1	64.5
Near OASPL (dB)	111.2	109.5	109.3	108.3	108.2
Near OASPL (dBA)	96.4	96.8	97.0	94.5	93.9
	Reference Propeller	HOPSE-1.3	HOPSE-2.6	HOPSE-3.9	HOPSE-6.5
Far OASPL (dB)	76.9	76.9	76.8	76.6	76.6
Far OASPL (dBA)	65.9	66.0	65.9	65.8	65.7
Near OASPL (dB)	111.2	110.0	109.4	108.9	108.7
Near OASPL (dBA)	96.4	96.9	97.3	94.7	94.3

For the cases considered it appears that as with in-plane sweep the greater the out-of-plane sweep the lower the noise. Based upon these predictions, the OPSE-6.5 configuration is recommended because it exhibits superior noise reduction characteristics than the reference case, i.e. it demonstrates significantly quieter noise characteristics in the far- and near-fields.

Manufacturing propellers with out-of-plane sweep is very difficult and large bending stresses are encountered. These stresses are generated due to the uneven radial mass distribution and centrifugal force effects. Straight bladed propellers are designed so that the radial mass distribution is on a straight radial line leading out from the hub and, therefore bending stresses due to centrifugal forces are avoided.

4.9 Propeller Design Using Natural-Laminar-Flow (NLF) Airfoils

Airfoil skin friction at high Reynolds numbers is significantly reduced by the successful design of airfoil shapes that exhibit large regions of laminar boundary layer flow on both the upper and lower surfaces [29,30]. Propellers are designed using these NLF airfoils in the hope that there is an increase in propeller efficiency due to the reduction of airfoil parasite drag. This study investigates NLF airfoils to determine if NLF propellers will exhibit lower noise characteristics than propellers using more conventional NACA airfoil sections.

Jeffrey Viken of Innovative Aerodynamic Technologies (IAT), an NLF design specialist, and designer of the NASA NLF(1)-0414F airfoil, designed a set of NLF airfoils for propellers based upon the same size and with the same performance characteristics as is used to design the reference propeller. [30] Based upon the sectional lift coefficient and Reynolds number distribution required as a function of blade radial position, Mr. Viken designed the NLF airfoils as labeled in Table 4.9.1 as a function of radial position r/R for the NLF propeller. Inspection of this table indicates a twist angle and sectional lift coefficient distributions very similar to that used for the reference propeller.

Table 4.9.1 Blade angles, chord and lift coefficient as a function of radial position for NLF propeller.

NLF Airfoil	r/R	r	c	t/c	β	α	c_l
ju-prop.20	0.10	3.80	6.50	0.1800	76.48	1.39	0.70
ju-prop.20	0.20	7.60	6.50	0.1800	61.70	1.39	0.70
ju-prop.40	0.30	11.40	6.50	0.1500	50.44	1.32	0.73
ju-prop.40	0.40	15.20	6.50	0.1500	42.15	1.32	0.73
ju-prop.55	0.55	20.90	6.50	0.1275	33.65	1.46	0.74
ju-prop.55	0.60	22.80	6.50	0.1275	31.46	1.46	0.74
ju-prop.70	0.70	26.60	6.50	0.1050	27.74	1.41	0.75
ju-prop.70	0.75	28.50	6.50	0.1050	26.22	1.41	0.75
ju-prop.70	0.80	30.40	6.50	0.1050	24.86	1.41	0.75
ju-prop.85	0.85	32.30	6.31	0.0825	23.10	1.01	0.58
ju-prop.85	0.90	34.20	5.72	0.0825	21.99	1.01	0.58
ju-prop.95	0.95	36.10	4.55	0.0675	20.51	0.65	0.42
ju-prop.95	0.975	37.05	3.59	0.0675	20.04	0.65	0.42
ju-prop.95	0.995	37.81	2.41	0.0675	19.69	0.65	0.42
ju-prop.95	1.00	38.00	1.98	0.0675	19.60	0.65	0.42

Examination of Table 4.9.1 reveals that the ju-prop.20 airfoil with a maximum thickness of 18%, is used at a r/R of 0.1 and 0.2, the ju-prop.40 with a t/c of 15% is used at a r/R of 0.3 and 0.4, the ju-prop.55 with a t/c of 12.75% at a r/R of 0.5 and 0.6, the ju-prop.70 with a t/c of 10.5% from a r/R of 0.7 to 0.8, the ju-prop.85 with a t/c of 8.25% at r/R of 0.85 and 0.9, and the ju-prop.95 with a t/c of 6.75% at r/R equal to and greater than 0.95. To gain insight into the unique shape of the NLF airfoil shapes, the NACA 44XX series and the ju-prop series are presented side by side in Figure 4.9.1 at various radial positions. For example, the NACA-4406 airfoil is plotted next to the ju-prop.95 airfoil both of which are used near the blade tip at a radial position of 0.95 r/R, noting that the NACA 44xx series airfoil is used on the reference propeller.

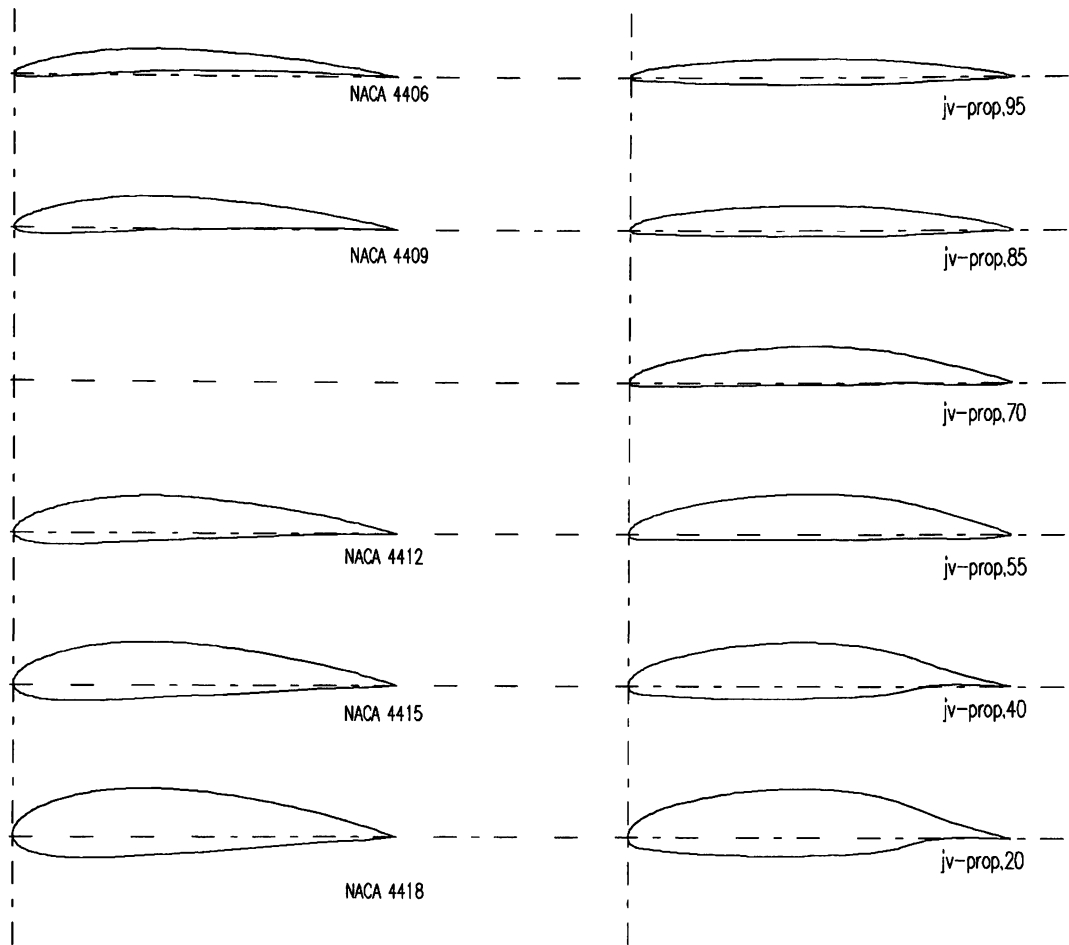


Figure 4.9.1 Comparison between NACA 44 and NLF series airfoils.

Figure 4.9.2 shows the propeller aerodynamic performance characteristics for the propeller with the NLF airfoils, where the thrust coefficient C_T , power coefficient C_P , and efficiency η are plotted as a function of advance ratio J . This propeller exhibits almost identical aerodynamic performance characteristics as the reference propeller. Both propellers are 76 in. diameter rotating at 2,400 rpm

at a cruise speed of 160 kts, resulting in a cruise advance ratio J of 1.07. Inspection of Figure 4.9.2 reveals a thrust coefficient C_T of 0.0447, power coefficient C_P of 0.0537, and efficiency of 88.7%. At standard sea-level conditions and level flight of 160 kts, these coefficients result in a power of 143.6 hp and 259.4 lb. compared to 145.0 hp, and 259.6 lb. at an efficiency of 87.9%. for the reference propeller. This comparison shows that the straight reference propeller exhibits similar thrust and power coefficient trends as the NLF propeller but the NLF propeller is 1% more efficient.

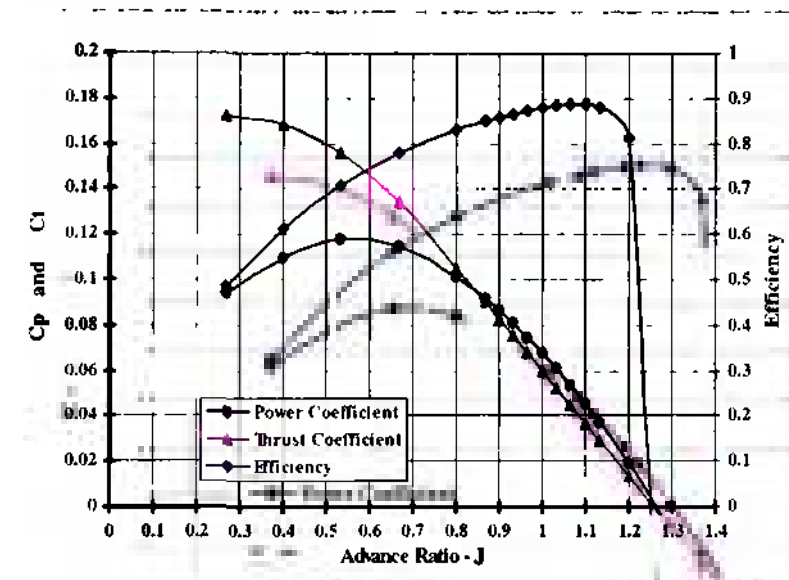


Figure 4.9.2 Aerodynamic Performance of Straight Propeller with NLF Airfoils

4.10 Noise Characteristics of NLF Propeller

Figure 4.10.1 shows the far-field unweighted OASPL levels for both the straight NLF and reference propellers for fly-over at an altitude of 1000 ft and a speed of 160 kts in steady level flight. Both propellers are rotating at 2,400 rpm.

The OASPL for both curves is nearly identical near and at the peak levels, but that the NLF propeller is slightly quieter during approach than the reference propeller and slightly noisier during the departure. Thus, for the unweighted case, there are no significant differences in the far-field OASPL between the NLF and reference propellers.

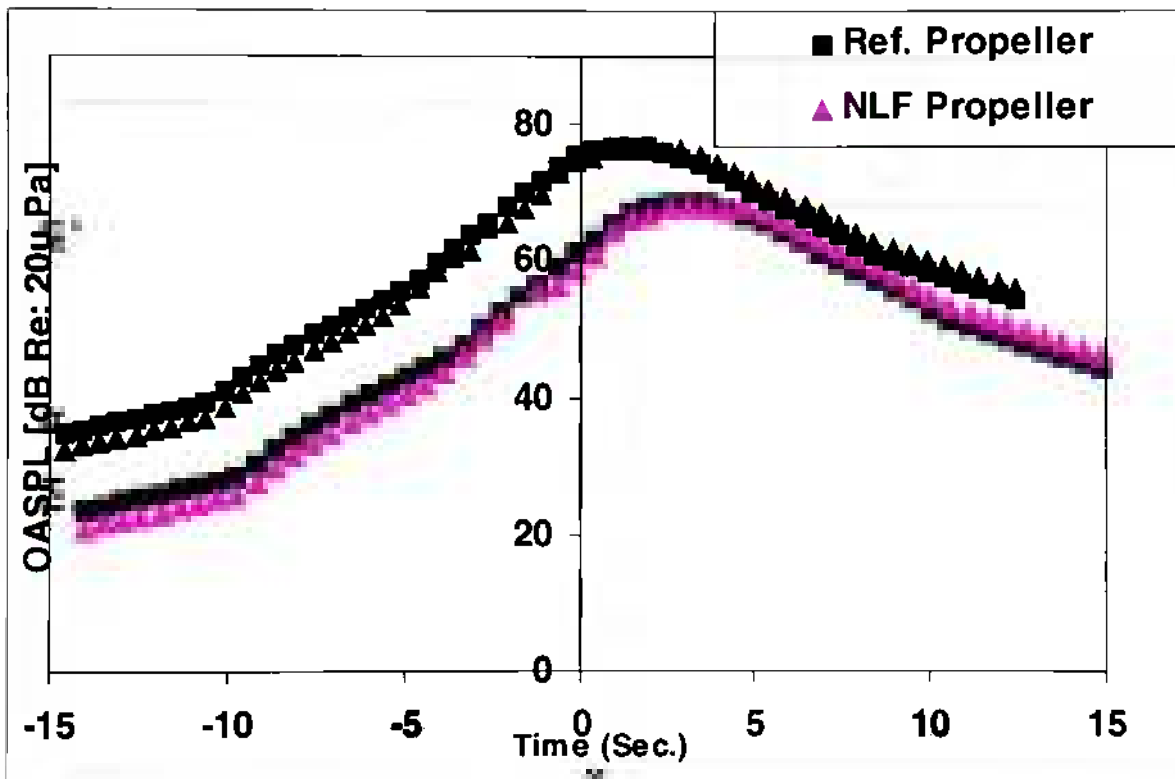


Figure 4.10.1 Fly-over Unweighted OASPL Far-Field Radiated Noise Characteristics of Straight NLF and Reference Propellers (2400 RPM).

The near-field unweighted SPL frequency spectrum of both the NLF and reference propeller's rotating at 2400 rpm is illustrated in Figure 4.10.2. Comparison of the data in the figure indicates that at BPF (harmonic number of one) the SPL for both propellers is

the same. However as the harmonic number increases in Figure 4.10.2 the SPL for the NLF propeller progressively increases over the reference propeller levels. This increase is most apparent at harmonic number of 20 (20BPF) where the SPL of the NLF propeller is approximately 7 dB greater than the reference propeller's SPL. As previously stated, thickness noise dominates the loading noise at the higher harmonics and comparing Table 4.2.1 with Table 4.9.1, shows that the thickness distribution as a function of radial position is different between the NACA 44 series and jv-prop (NLF) airfoil sections. Review of Figure 4.9.1, where sketches of both the NACA 44 series and the jv-prop airfoils are shown at various radial positions, there are significant volume differences between the two airfoil series. Because of these geometrical differences, it is not surprising that the thickness noise is significantly different and is the reason why the SPL at the higher harmonics is greater in the NLF propeller than the reference propeller.

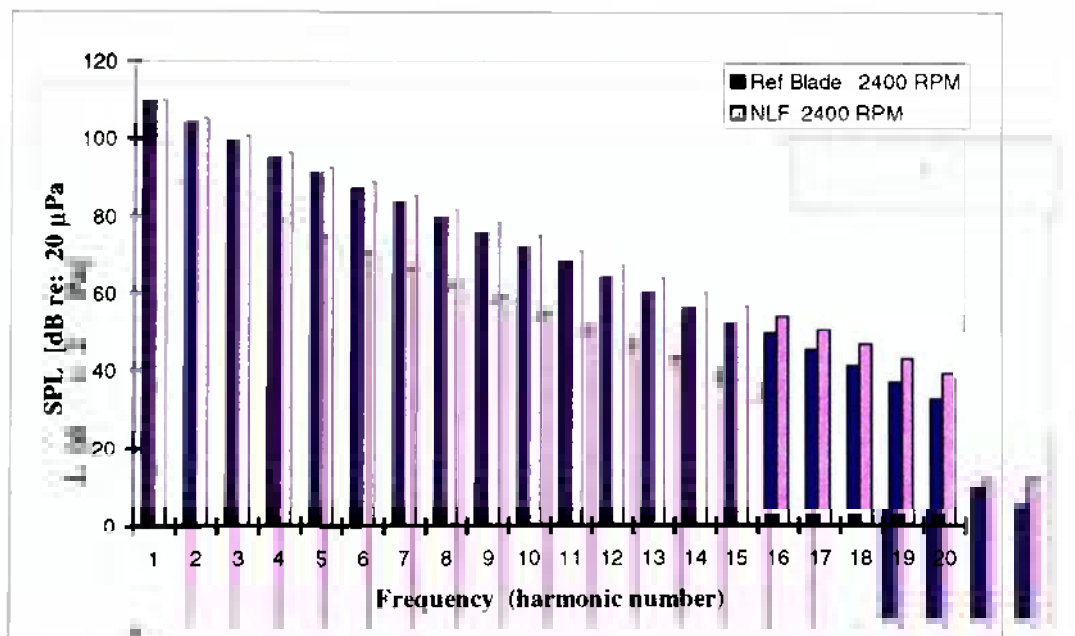


Figure 14.10.2 Frequency Distribution of Near-Field Unweighted SPL for the NLF Propeller and the Reference Propeller rotating at 2,400 RPM and at Directivity Angle of 105°.

A-weighted noise levels are important in noise research in that A-weighted levels allow sound levels to be adjusted to represent the response of the human ear. Table 4.10.1 is presented to show the unweighted and A-weighted OASPL for maximum fly-over and near-field levels at a directivity angle of 105°, for the straight NLF and reference propeller as well as the HIPSE-6.5, OPSE-6.5 and the swept NLF propellers (NFL-HIPSE-6.5, NLF-OPSE-6.5). The HIPSE-6.5 and the in-plane swept NLF-HIPSE-6.5 propeller are swept identically with 6.5 in. of sweep in the plane of rotation, starting at the 0.5 r/R radial position. Similarly the OPSE-6.5 and NLF-OPSE-6.5 are swept identically, with the out-of-plane sweep beginning at the 0.2 r/R radial position with 6.5in of tip sweep aft of the plane of rotation.

Table 4.10.1 Non-weighted and A-weighted OASPL for Maximum Fly-Over and Near-Field Levels (at a Directivity Angle of 105°), for NLF and Reference Propeller's for straight, in and out-of- plane swept configurations.

	Reference Propeller	HIPSE-6.5	OPSE-6.5
Far OASPL (dB)	76.9	75.9	75.1
Far OASPL (dBA)	65.9	64.6	64.5
Near OASPL (dB)	111.2	110.7	108.2
Near OASPL (dBA)	96.4	95.0	93.9
	NLF Propeller	NLF-HIPSE-6.5	NLF-OPSE-6.5
Far OASPL (dB)	77.1	76.3	75.6
Far OASPL (dBA)	66.1	63.7	63.7
Near OASPL (dB)	111.7	111.3	108.9
Near OASPL (dBA)	97.6	96.5	93.6

The aerodynamic performance characteristics C_T , C_P , and η of all six propeller configurations are within 2.2% of one another. Inspection of Table 4.10.1 indicates that the unweighted far-field OASPL of the reference propeller is 76.9 dB and the unswept NLF propeller is 0.2 dB noisier while the HIPSE-6.5 and NLF-HIPSE-6.5 propellers are respectively 1.0 dB and 0.6 dB quieter. The far-field A-weighted OASPL of the reference propeller is 65.9 dBA and the unswept NLF propeller is 0.2 dBA noisier while the HIPSE-6.5 and NLF-HIPSE-6.5 propellers are respectively 1.3 dBA and 2.2 dBA quieter, i.e. both in-plane swept configurations are significantly quieter than either swept configuration when comparing the A-weighted levels. The near-field differences are not as significant. The NLF propeller swept in-plane generates the same A-weighted levels as the reference propeller and the HIPSE-6.5 is 1.5 dBA quieter. When swept out of plane the far-field OASPL for the OPSE6.5 is 1.8 dB quieter than the reference propeller while the NLF-OPSE-6.5 is 1.3 dB quieter. The far-field A-weighted OASPL for OPSE-6.5 and NLF-OPSE-6.5 is 1.4 and 2.2 dBA quieter than the reference propeller respectively. When swept out-of-plane radiated noise in the near field results in even greater noise reduction. OPSE-6.5 is 3dB (2.5dBA) quieter than the reference propeller in the near field and NLF-OPSE-6.5 is 2.3dB (2.7dBA) quieter than the reference propeller. These comparisons indicate that both the HIPSE-6.5 and NLF-HIPSE-6.5 propellers are generally quieter and that their A-weighted levels are significantly quieter, than the reference propeller. Also, the OPSE-6.5 and NLF-OPSE-6.5 have quieter far-field A-weighted levels and their near-field noise radiation is significantly quieter than

the reference propeller in both unweighted and A-weighted levels. In general there is no significant acoustical advantage using NLF airfoils for propellers when compared to NACA 44XX series airfoils.

4.11 Optimal Propeller Design

The optimal propeller in this study is derived from a combination of the of the aforementioned design parameters. The optimal blade is designed to rotate at 2400 rpm to avoid shock wave formation at the tip. The propeller has an elliptical tip shape for ease in manufacturing and good noise characteristics. Fundamentally the blade is designed for optimum efficiency with the basic characteristics of the straight NLF propeller with NLF airfoils, which provide optimal efficiency as well as good A-weighted noise characteristics. Incorporated into the design is both in- and out-of-plane sweep equivalent to the sweep used in NLF-HIPSE-6.5 and NLF-OPSE-6.5 configurations. The in and out of plane sweep are incorporated for near- and far-field noise reduction.

Figure 4.11.1 Illustrates the Far-field unweighted OASPL levels for the optimal propeller compared to the reference propeller for fly-over at an altitude of 1000 ft and a speed of 160 kts in steady level flight. Both propellers rotate at 2400 rpm, with the same thrust. The OASPL for both curves is nearly identical near and at the peak levels, but that the NLF propeller is slightly quieter during approach than the reference propeller and nearly identical during the departure.

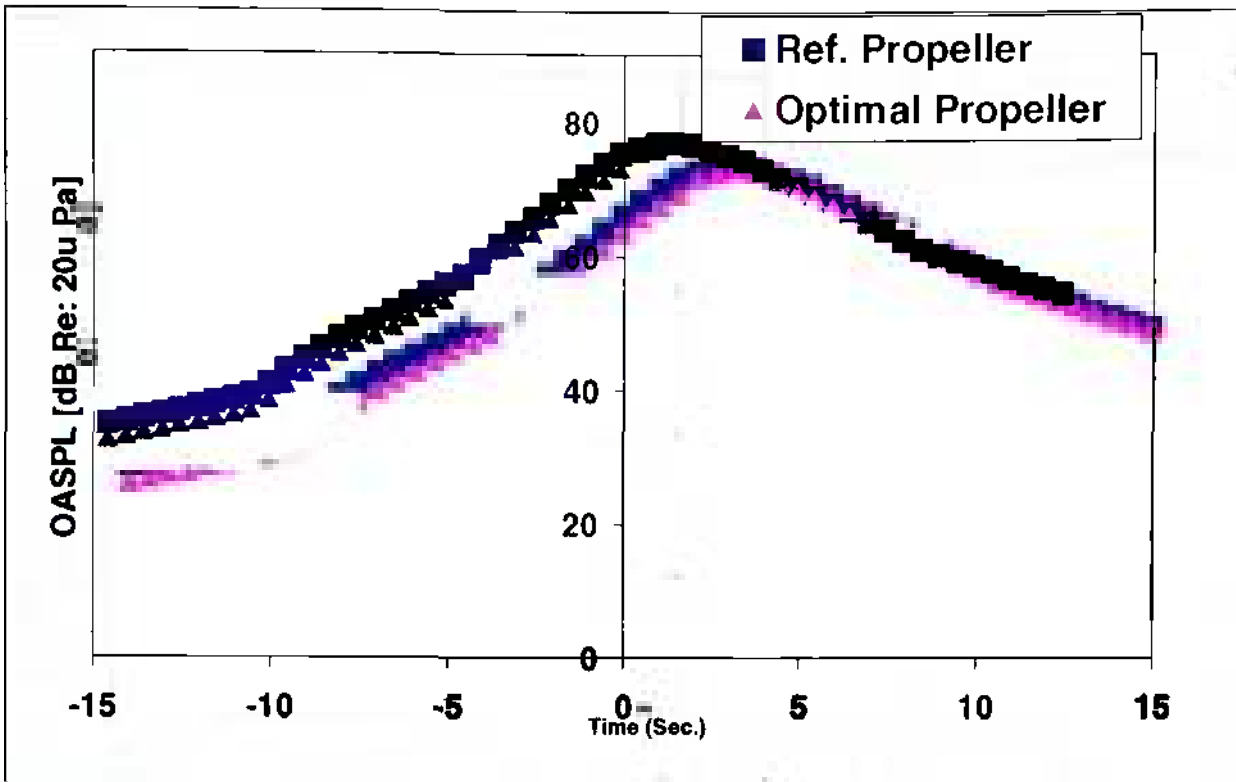


Figure 4.11.1 Fly-over Unweighted OASPL Far-Field Radiated Noise Characteristics of the Reference and Optimal Propellers (2400 RPM).

The optimal propeller thrust coefficient C_T of 0.0448, power coefficient C_P of 0.0539, and efficiency of 88.9% compared to 88.7% for the straight NLF propeller. Aerodynamically the optimal propeller has almost identical performance characteristics to the straight NLF propeller.

Table 4.11.1 illustrates the radiated noise characteristics of the optimum propeller as compared to the reference and straight NLF propeller's. When compared to the reference propeller, far-field radiated noise is decreased by 1.1 dB and 3.6 dBA for the optimal propeller. Under the same comparison, the

near-field noise characteristics of the optimal propeller are decreased by 1.7 dB and 2.3 dBA over the reference propeller levels. Since the optimal propeller design is based on the straight NLF propeller, it is important to note that noise reduction over the straight NLF blade is 1.3 dB (3.8 dBA) in the far-field, and 2.2 dB (3.5 dBA) in the near field.

Table 4.11.1 Non-weighted and A-weighted OASPL for Maximum Fly-Over and Near-Field Levels (at a Directivity Angle of 105°), for the Reference, Straight NLF and the Optimal propellers.

	Reference Propeller	NLF Propeller	Optimal Propeller
Far OASPL (dB)	76.9	77.1	75.8
Far OASPL (dBA)	65.9	66.1	62.3
Near OASPL (dB)	111.2	111.7	109.5
Near OASPL (dBA)	96.4	97.6	94.1

Therefore, optimizing the design parameters in this study resulted in a the optimal propeller design which is slightly quieter overall with significant noise reduction in the A-weighted spectrum and is 1% more efficient than the reference propeller.

4.12 Unsteady Blade Loading

It is important to note that most acoustic prediction methods make predictions for propellers operating under ideal conditions. Obviously in actual practice, ideal conditions are the exception rather than the rule. While in flight,

the propeller shaft is often at an angle of attack and this angle causes flow distortion or unsteady loading on the propeller. Therefore the blade loading varies through its revolution as a cyclic change in local angle of attack. Unsteady loading on the blade increases the noise produced by the propeller [4]. Therefore, propeller noise prediction methods must consider effects of unsteady blade loading in order to accurately predict the noise generated by the propeller under investigation.

Recent updates to ANOPP-PAS include the effects of unsteady blade loading due to propeller inflow angle on the noise generated by propellers. [30] In this study, the updated ANOPP-PAS code is utilized to determine unsteady loading effects on the two bladed reference propeller radiated noise characteristics. The reference propeller is simulated to be operating with a relative propeller angle of attack of five degrees.

Figure 4.12.1 represents the overall near-field SPL at directivity angle 75° of the reference propeller under steady and unsteady loading conditions. The overall SPL is the sum of the loading and thickness noise components. Both flight conditions generate similar data sets that decrease with increasing harmonic number. As anticipated, the SPL generated under the unsteady loading condition is higher than the steady loading case at most harmonic numbers. At a directivity angle of 75° the difference in OASPL is 2.9 dB: the unsteady condition is 112.9 dB versus 110.1 dB for the steady condition. At blade

passing frequency the difference is even greater with the unsteady case some 3.6 dB higher than the steady condition. The reference blade under steady conditions has peak OASPL values of 111.2 dB at 105° directivity versus 112.9 at 75° for the unsteady loading case. Thus, at their respective noisiest locations the blade operating in unsteady conditions is predicted to be 1.7 dB (2.7 dBA) louder than the propeller under steady loading conditions.

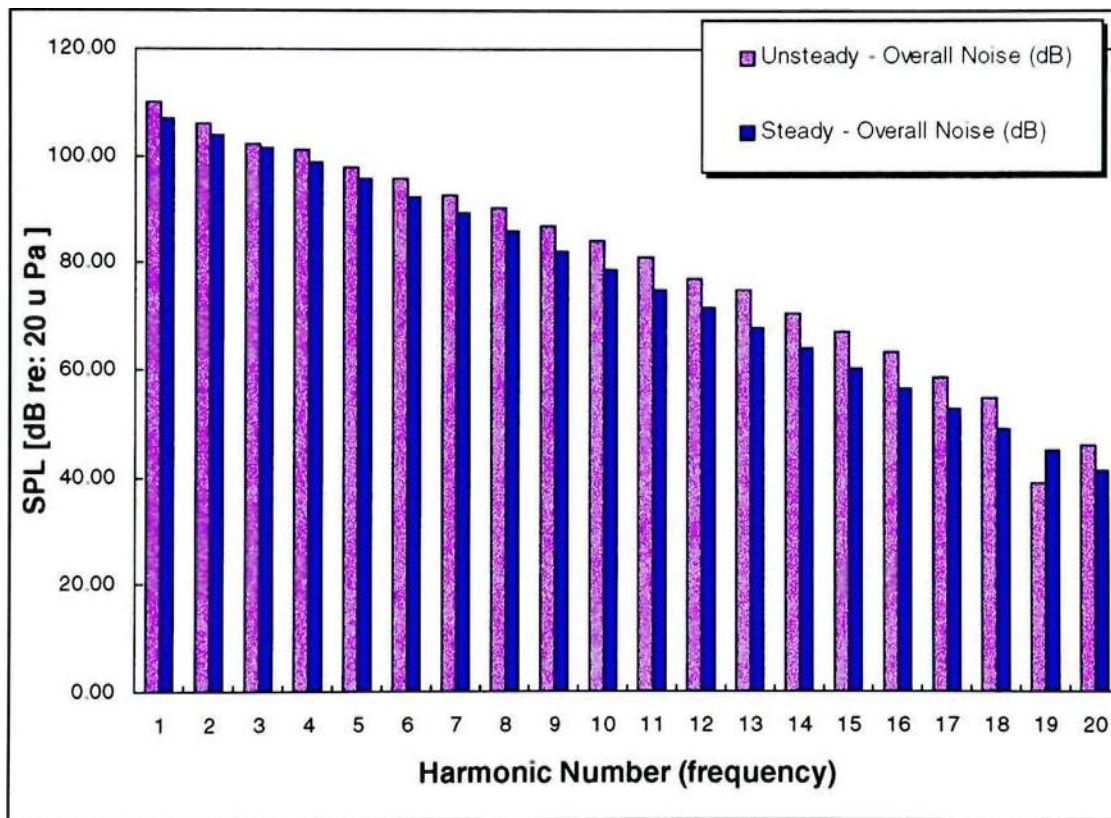


Figure 4.12.1 Comparison of Unsteady and Steady Overall Noise generated by Reference Propeller [SPL (dB Re: 20 μ Pa) vs. Harmonic Number (f)].

As the previous data indicates, unsteady blade loading has an impact on the radiated noise characteristics of the reference propeller. The impact to far-

field characteristics is especially large as shown in the far-field radiated noise characteristics of the reference blade under steady and unsteady loading conditions, shown in Figure 4.12.2. Under unsteady loading conditions the reference blade has a maximum OASPL of 79 dB (67dBA). Acoustic theory predicts a peak approximately one second past the observer, as seen in the steady loading case. The unsteady loading level occurs 0.39 seconds past the observer. Additionally theory predicts that the approach levels should be lower than levels during the retreat phase, the unsteady case has nearly identical levels during the approach and retreat phases. The most dramatic impact of the unsteady loading occurs 15 seconds before reaching the observer, when the difference between the steady and unsteady case is an enormous 22 dB. This large difference between levels monotonically declines to almost zero at the observer when the levels become almost identical throughout the retreat phase. Thus, unsteady loading can have a significant impact on actual radiated noise characteristics of propellers, particularly in the far-field.

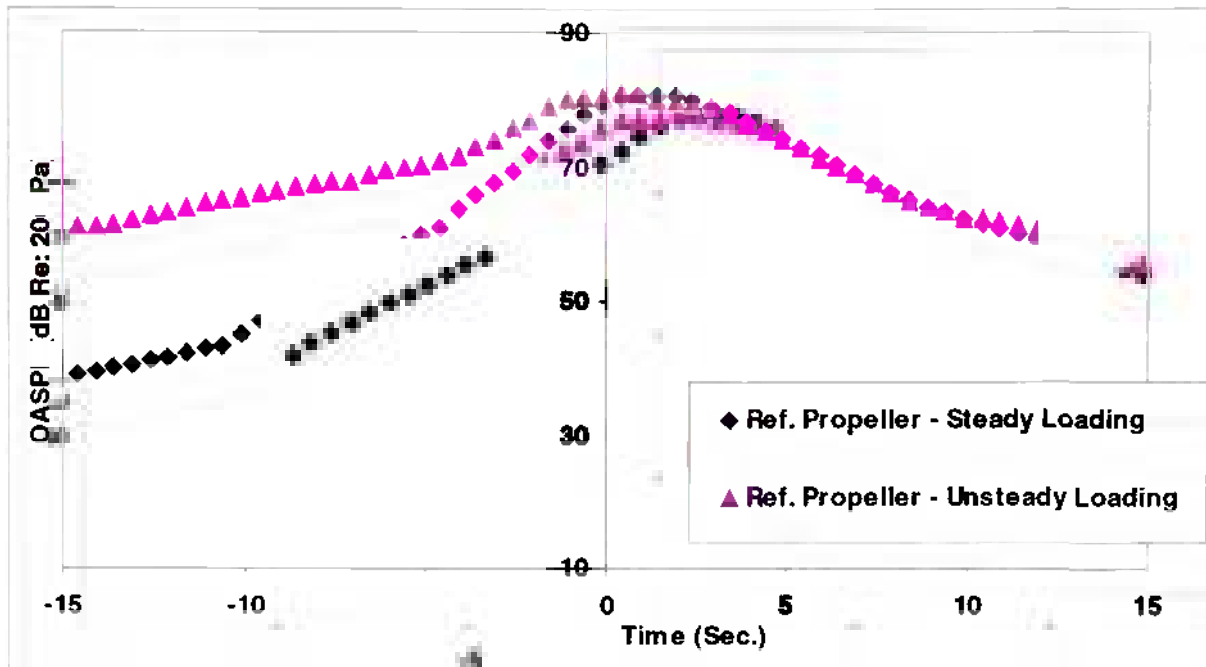


Figure 4.12.2 Comparison of Unsteady and Steady Far-Field Radiated Noise At 1000ft [OASLP dB Re: 20 μ Pa vs. Time (Sec)]

In Figure 4.12.3 the near-field thickness noise versus harmonic number (frequency) is plotted under both steady and unsteady loading conditions for the reference propeller at directivity angle of 75° . Inspection of this figure reveals that the thickness noise is greater for the unsteady loading conditions than steady loading over all harmonics. Though the trend of the data is similar to the overall noise characteristics, it is evident that the difference in that the thickness noise increases with increasing harmonic number.

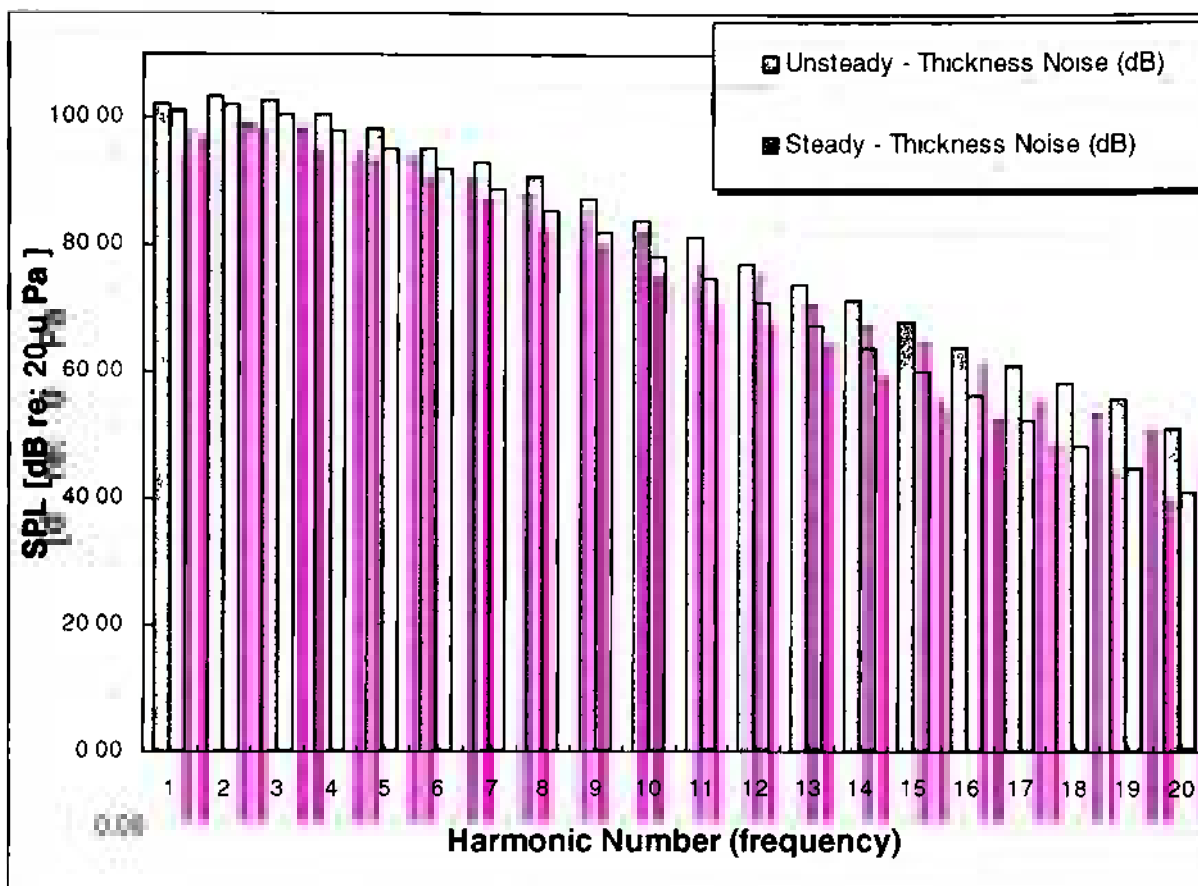


Figure 4.12.3 Comparison of Unsteady and Steady, Near-Field Thickness Noise Generated by the Reference Propeller [SPL (dB Re: 20 μ Pa) vs. Harmonic Number (f)].

Figure 4 12.4 shows a comparison of the steady and unsteady loading noise generated by the reference propeller. Inspection of this figure indicates that the greatest difference between steady and unsteady loading conditions occur for the loading noise component. As shown in the previous charts, the loading noise decreases with increasing harmonic number until the ninth harmonic when the

unsteady loading condition levels off and remains nearly constant and at fairly high levels through the remaining harmonics.

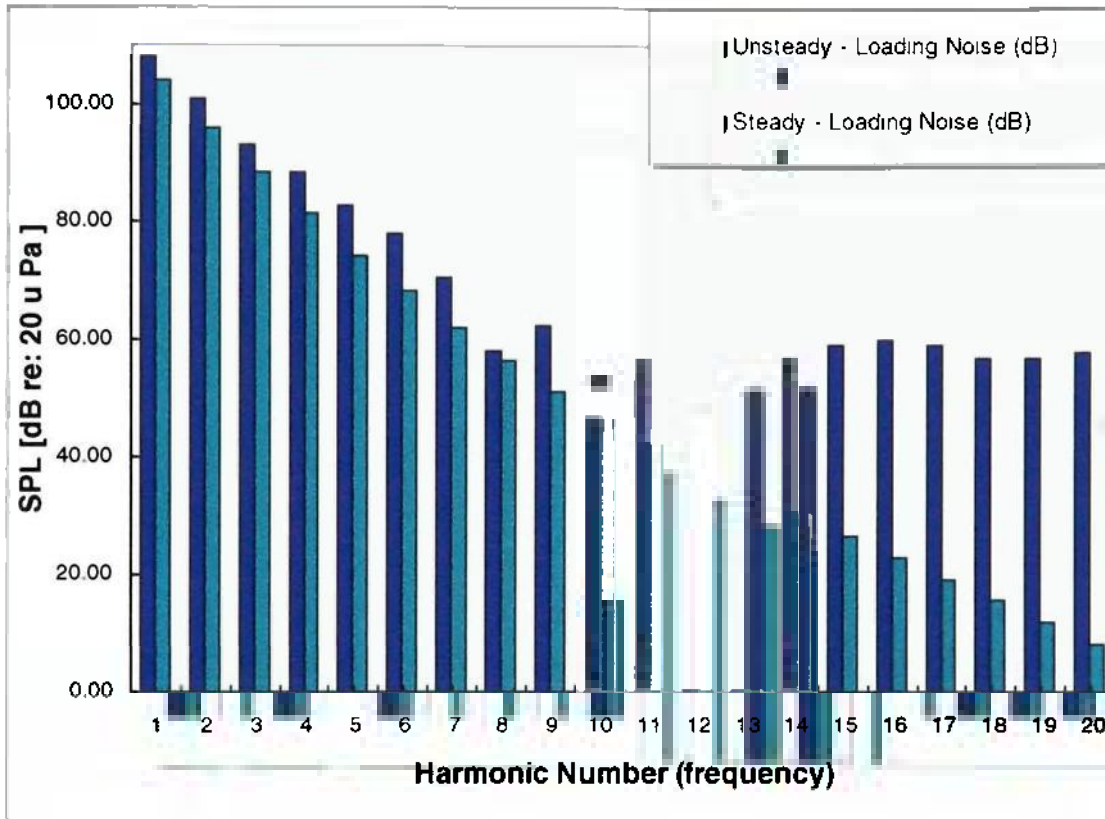


Figure 4.12.4 Comparison of Unsteady and Steady Loading Noise Generated by the Reference Propeller [SPL(dB Re: 20 μPa) vs. Harmonic Number (f)].

As seen in the Figures 4.12.2 – 4.12.4, the unsteady loading conditions increase both the near-field thickness and loading noise components generated by the propeller and therefore increase the overall noise generated by the propeller. Figure 4.12.5 shows a comparison of the near-field overall noise directivity patterns for the steadily and unsteadily loaded reference propeller. The changes in noise radiation due to unsteady load have an impact on the directivity pattern, as seen in reviewing Figure 4.12.5.

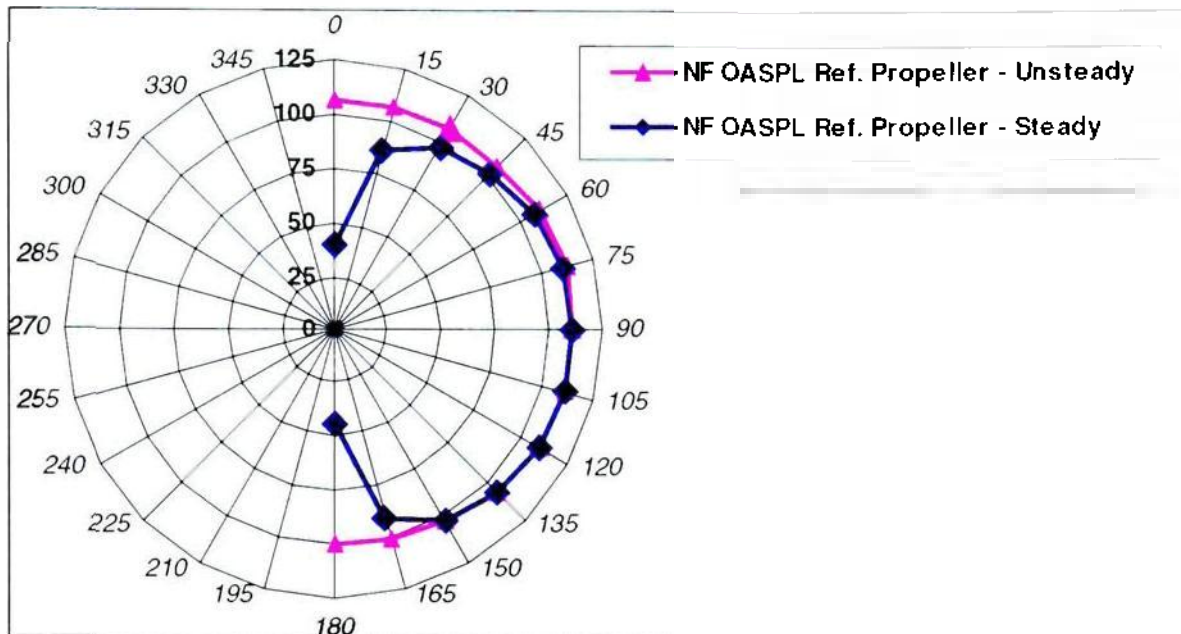


Figure 4.12.5 Comparison of Unsteady and Steady Near-Field Overall Noise Directivity Patterns [Near Field OASPL Re: 20 μ Pa as a function of Directivity Angle].

Inspection of Figure 4.12.5 reveals that the reference blade under steady conditions has a peak OASPL value of 111.2 dB at 105° directivity angle versus 112.9 dB at 75° for the unsteady loading case. At 0° and 180° the OASPL for steady loading is less than 50 dB but for unsteady loading the OASPL is greater than 100 dB. The directivity angle illustrated in Figure 4.4.2 is measured aft of the propeller looking forward as follows: forward of the propeller is zero; 90° is measured in the plane of the propeller's rotation and directly aft is 180°

In addition to the maximum radiation location shift, the unsteady condition directivity pattern is almost constant from 0° to 180°. Though the range the

unsteady OASPL ranges from 106.3 dB at zero to 112.9 at 75, a delta of 6.6 dB. By comparison the steady loading case varies 72 dB from maximum to minimum at 105° and 0° respectively.

As the previous data indicates, unsteady blade loading has a major impact on the radiated noise characteristics of the reference propeller. Shown in Figure 4.12.6 are the steady and unsteady far-field radiated noise characteristics. The impact to far-field characteristics is shown to be especially large for the reference blade during approach, as predicted by acoustic theory. Under unsteady loading conditions the reference blade has a maximum OASPL of 79 dB (67dBA). The unsteady loading peak level occurs 0.39 seconds past the observer. Traditional steady loading acoustic theory predicts a peak approximately one second past the observer, as shown in the steady loading case. The unsteady and steady cases have nearly identical noise levels as the propeller passes and retreats from the observer. Unsteady loading levels are greatest 15 seconds before reaching the observer, when the difference between the steady and unsteady levels is an enormous 22 dB. This large delta between levels steadily declines to almost zero at the observer when the levels become almost identical throughout the retreat phase. Thus, unsteady loading can have a significant impact on actual radiated noise characteristics of propellers, particularly in the far-field during the approach phase.

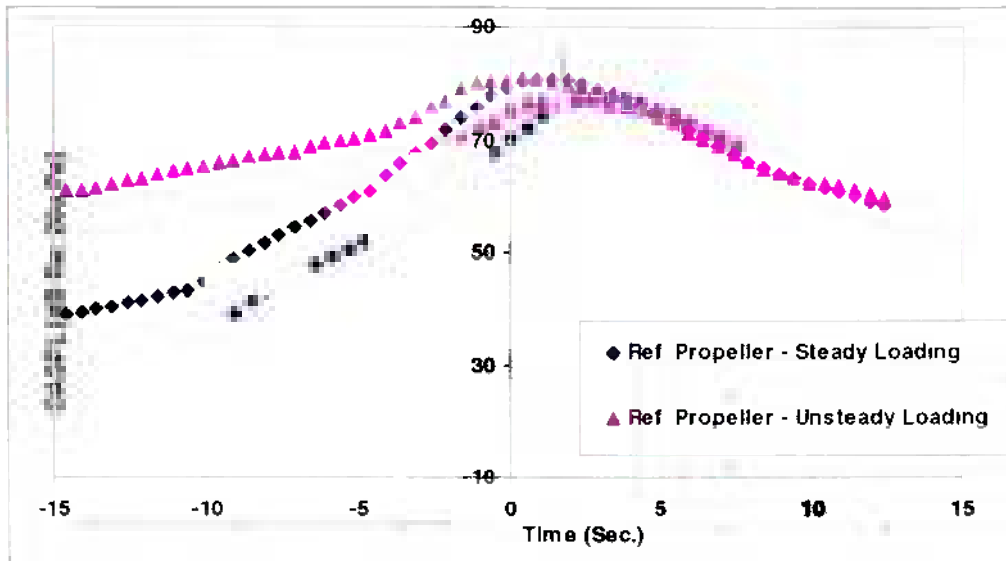


Figure 4.12.6 Comparison of Unsteady and Steady Far-Field Radiated Noise At 1000 ft [OASLP dB Re: 20 μ Pa vs. Time (Sec)]

5.0 Conclusions

The NASA Aircraft Noise Prediction Program-Propeller Analysis System (ANOPP-PAS) was used to design quiet two-bladed general aviation (GA) propellers. This theoretical investigation resulted in the following conclusions:

- Based upon noise and manufacturing considerations, the elliptical blade tip shape was deemed best tip design when compared with square, parabolic and circular tips, even though the parabolic tip was predicted to be the quietest.
- Using propeller rotational speeds of 2700 rpm for a 76 in. diameter 2-bladed propeller, will always result in extremely high radiated noise levels because of shock wave formation at the blade tip and this excessive noise problem does not occur at 2400 rpm due to reduced tip Mach numbers.
- Using in-plane sweep on the 76 in. diameter 2-bladed propeller, resulted in a predicted far-field OASPL reduction of 0.6 dB and 2.2 dBA, and near-field OASPL reduction of 0.5 dB and 1.4 dBA when compared to the typical straight 2-bladed propeller of the same diameter. Both propellers rotated at 2,400 rpm and were designed using NACA 44XX series of airfoils.
- Using natural-laminar-flow (NLF) airfoil shapes for a 76 in. diameter and straight 2-bladed propeller, resulted in a one percent increase in propeller efficiency and slight increases in the near- and far-field OASPL when compared to the straight 2-bladed propeller using NACA 44XX series of airfoils. Both propellers were of the same diameter and rotating at 2,400 rpm.
- A 2-bladed propeller with in-plane sweep with NACA 44 series and NLF airfoil shapes, resulted in approximately the same near- and far-field non-weighted noise levels as for the straight 2-bladed propeller with the same airfoils. However when compared to the reference blade, the A-weighted levels for the in-plane swept blades, resulted in significant noise reduction of 1-2 dBA. These propellers were of the same 76 in. diameter and were both rotated at 2400 rpm.

- Using out-of-plane sweep on the 76 in. diameter 2-bladed propeller, resulted in a predicted far-field OASPL reduction of 1.8 dB and 1.4 dBA, and near-field OASPL reduction of 3.0 dB and 2.5 dBA when compared to the typical straight 2-bladed propeller of the same diameter. Both propellers rotated at 2,400 rpm and were designed using NACA 44XX series of airfoils.

- A 76 in. optimal propeller was designed with NLF airfoils, in-plane and out-of-plane sweep and elliptical tip shape. The optimal propeller was 1% more efficient than the reference propeller. Additionally, the optimal design resulted in a predicted far-field OASPL reduction of 1.1 dB and 3.6 dBA, and a near-field OASPL reduction of 1.7 dB and 2.3 dBA when compared to the straight bladed reference propeller.

6.0 Recommendations

Anechoic wind tunnel tests should be performed to validate the design and radiated noise prediction capability of the NASA Aircraft Noise Prediction Program-Propeller Analysis System (ANOPP-PAS). The propeller designs used in this investigation should be used in performing anechoic wind tunnel tests to verify the predicted propeller aerodynamic performance and radiated noise characteristics. These model tests would also be used to develop and verify the radiated noise scaling laws for use in full-scale evaluations. Propeller aerodynamic scaling laws are reasonably well understood but this is not the case for radiated noise characteristics. Anechoic wind tunnel tests in conjunction with the theoretical prediction capabilities of the ANOPP-PAS computer code will allow the development of accurate propeller radiated noise scaling laws. This recommended validation will result in the ability of General Aviation (GA) aircraft and propeller manufacturers to use the ANOPP-PAS computer code to design quiet and efficient propellers with a reasonable degree of accuracy and confidence.

These anechoic wind tunnel tests should also investigate propeller installation effects. The ANOPP-PAS computer code has limited capability of

predicting unsteady blade loading due to in part to installation effects; therefore, a simplified nacelle installation algorithm should be developed and incorporated into the code. Incorporating this capability will greatly strengthen the ANOPP-PAS computer code capabilities. ANOPP's ability to predict noise due to unsteady blade loading should be further examined and results should be compared with flight data.

Further in-plane and out-of-plane sweep designs should also be studied to determine the full capability of using sweep to reduce radiated noise characteristics for GA aircraft propellers. These future studies must look carefully at the practicality of manufacturing highly swept-propeller blades as well as the strength characteristics. It is easy to envision a case where a highly swept propeller is designed that is efficient and quiet but would experience blade failure because of inadequate strength capabilities.

REFERENCES

- [1] Rathgelber, R. K., and Sipes, D. E., "The Influence of Design Parameters on Light Propeller Aircraft Noise," SAE-770444, 1977.
- [2] Wilson, "Noise Control, Measured Analysis, and control of Sound and Vibration"
Malabar, Fl: Kreiger Publishing, 1994
- [3] Metzger, F. B., "An Assessment of Propeller Aircraft Noise Reduction Technology," NASA CR 198237, August 1995.
- [4] Klatte, R.J. and Metzger, F.B. "Influence of Noise Reduction on Weight and Cost of general Aviation Propellers." FAA-AEE-79-18, June 1979.
- [5] Hubbard, H. H., "Aeroacoustics of Flight Vehicles: Theory & Practice," NASA RP-1258, 1991.
- [6] Chusseau M., Roozen E., Pauzin S., Matharan P., Carrere A., "Light Aircraft propeller: Design Parameter Effects on Acoustics and Aerodynamics," AIAA 93-4443, October 1993.
- [7] Rawls, John W., Jr., "10.2 Blade Shape Module. Aircraft Noise Prediction Program Theoretical Manual, Propeller Aerodynamics and Noise." William E. Zorumski and Donald S. Weir, eds., NASA TM-83199, Part3, June 1986.
- [8] Meacock, F.T., *The Elements of Aircraft Propeller Design*. London: E&F. Spon LTD, 1947
- [9] Mises, Richard Von, "Theory of Flight," New York: Dover Publications, 1959
- [10] Weick, fred E. Aircraft Propeller Design. New york and London: McGraw-Hill, 1930

References Continued

- [11] Patrick, H.V.L., "*Aeroacoustics Graduate Seminar Notes*" Embry-Riddle Aeronautical University, Spring 1995
- [12] Goldstein, M.E., "Aeroacoustics", NASA SP-346, 1974
- [13] Fowcs Williams, J. E. and Hawkings, D. L., "Sound Generation of Turbulence and Surfaces in Arbitrary Motion," *Philos. Trans. R. Soc. London, Ser. A.*, Vol. 264, 1969.
- [14] Lighthill, M. J., "On Sound Generated Aerodynamically: I. General Theory," *Proc. R. Soc. London, Ser. A*, Vol. 211, 1952, pp. 564-587.
- [15] Metzger, F. B., "A Review of Propeller Noise Prediction Methodology 1919-1994," NASA CR 198156, June 1995.
- [16] Farassat, F., "Generalized Functions and Applications to Aeroacoustics Seminar", NASA Langley Research Center, August 1996.
- [17] Gutin, L., "On Sound Field of a Rotating Propeller", NASA TM 1195, October 1948.
- [18] Brentner, K.S. "Prediction of Helicopter Rotor Discrete Frequency noise", NASA TM 87721, October 1986
- [19] Padula, Sharon L., " 11.1 Subsonic Propeller Noise Module, Aircraft Noise Prediction Program Theoretical Manual, Propeller Aerodynamics and Noise." William E. Zorumski and Donald S. Weir, eds., NASA TM-83199, Part 3, June 1986.
- [20] McCormick, Barnes Warnack, *Aerodynamics: Aeronautics and Flight Mechanics*. John Wiley and Sons, 1979
- [21] Succi, G. P., "Design of Quiet Efficient Propellers," SAE Tech. Paper 790584, 1979.
- [22] Nguyen, L. Cathy, " A users Guide for the NASA ANOPP Propeller Ananalysis System," NASA Contractors Report, Contract NAS1-96014, 1996
- [23] Jacobs and Pinkerton, "Tests of NACA Airfoils in the Variable Density Wind Tunnel", Series 44 and 64" NACA TN-401, 1931

References Continued

- [24] Farassat, F., "The Unified Acoustic and Aerodynamic Prediction Theory of Advanced Propellers in the Time Domain," AIAA J., Vol.24,1986, pp. 578-584.
- [25] Borst, Henry V., Volume 1, "Aerodynamic Performance and Installation", USAAMRDL TR-73-34A, 1973.
- [26] Dwinell, J. D., "Principles of Aerodynamics," McGraw-Hill, 1949
- [27] Richards, E. J., and Mead, D. J., "Noise and Acoustic Fatigue in Aeronautics," Wiley, 1968.
- [28] Farassat, F., Consultation Conversation Fall 1996
- [29] Hanson, D. B., "Compressible Helicoidal Surface Theory for Propeller Aerodynamics and Noise," AIAA J. Vol. 18, pp. 1213-1220.
- [30] Keiter, I.D., "Impact of Advanced Propeller Technology on Aircraft/ Mission Characteristics of Several General Aviation Aircraft," SAE Technical Paper No. 810584, April 1981.
- [31] McGhee, R.J., Viken, J.K., Pfenninger, W., Beasley, W.D. and Harvey, W.D.: "Experimental Results for a Flapped Natural Laminar Flow airfoil with High Lift/ Drag Ratios," NASA TM-85788, 1984.
- [32] Sewall, W.G., McGhee, R.J., Viken, J.K., Waggoner, E.G., Walker, B.S. and Millard, B.F.: "Wind Tunnel Results for a High-Speed, Natural Laminar Flow Airfoil Designed for General Aviation Aircraft," NASA TM-87602, 1985.
- [33] Kelly, Jeffery J., Nguyen, L. Cathy, "Influence of Shaft Angle of Attack on Sound Radiation by Subsonic Propellers", Submittal to AIAA Journal of Aircraft, October 1996.